Research article

Genome-wide analysis of the non-coding RNA synthetic genetic network reveals extensive plasticity and unique phenotypes in yeast

Running title: Mining yeast non-coding RNA synthetic interactions

Marcin G Fraczek[#,1,2], Soukaina Timouma[#,1,2], Laura Natalia Balarezo-Cisneros[#,1,2], Steven Parker[1,2], Kobchai Duangrattanalert[1], Matthew Wenjie Feng[2], Sam Griffiths-Jones[2], Raymond T O'Keefe*[,2] and Daniela Delneri*[,1,2]

[#]Joint authorship

[1]Manchester Institute of Biotechnology, Faculty of Biology, Medicine and Health, The University of Manchester, Manchester, United Kingdom

[2]Division of Evolution, Infection and Genomics, Faculty of Biology, Medicine and Health, The University of Manchester, Manchester, United Kingdom

*Corresponding authors: d.delneri@manchester.ac.uk; rokeefe@manchester.ac.uk

Running title: Analysis non-coding RNA synthetic interactions in yeast

ABSTRACT

Recent studies identified non-coding RNAs (ncRNAs) with unknown function that are responsible for major fitness changes in yeast. To understand ncRNA interplay and aid their functional assignment, the synthetic genetic array (SGA) methodology was employed to create >15,000 double mutants and to score their epistasis in different environments. Unlike the protein network, ncRNAs mostly displayed positive epistasis in rich medium. Interestingly, the negative interactions significantly increased under stressors, showing environmental-dependent functions for ncRNAs. No correlation was found between the network of ncRNAs and that of their neighbouring genes, suggesting functional independence. The U3 paralogs, SNR17A and SNR17B, share the majority of genetic interactions in rich medium as expected. For example, SUT480 interacted with both paralogs and its function was linked to 18S rRNA processing. However, under stressors, a large number of unique epistatic interactions were observed, supporting the notion that SNR17A and SNR17B have diverged and sub-functionalised after genome duplication.

INTRODUCTION

The majority of biological processes in the cell are performed by proteins, either independently or by interactions with other proteins. However, eukaryotic genomes pervasively transcribe sequences producing a wide range of non-coding RNAs (ncRNAs), which although are not translated into proteins, have important and often essential roles in the cell (*1-3*). Besides the well-known rRNAs and tRNAs, other classes of ncRNAs exist in eukaryotic cells. Approximately 98% of the human genome consists of non-protein-coding DNA sequences that were once regarded as non-functional evolutionary leftovers (*4*). In fact, most of the genome is transcribed and a number of ncRNAs are regulatory assisting in essential cellular processes, such as for example regulation of gene expression and transcription, apoptosis, telomere maintenance or RNA processing (*1-4*). Since ncRNAs are integral components of cellular regulatory networks, it is not surprising that many diseases in humans, ranging from cancer to neurological disorders, are affected by mutations or defects in many of these ncRNAs (*5*).

In *Saccharomyces cerevisiae*, approximately 85% of the genome is pervasively transcribed producing ~25% non-coding and ~75% protein-coding transcripts (*6*). *S. cerevisiae* constitutes an exception among Eukaryotes as it has lost small regulatory ncRNAs and conserved proteins required for RNA interference (RNAi) such as Argonaute and Dicer-like RNAses (*7, 8*). However, several classes of so called classical or housekeeping ncRNAs are present in the *S. cerevisiae* genome including tRNAs and rRNAs involved in protein synthesis as well as small nuclear RNAs (snRNAs) known to perform intron splicing and small nucleolar RNAs (snoRNAs) that process or direct chemical modifications of other RNAs. Novel functions for these classical ncRNAs are still emerging. Furthermore, a great number of ncRNAs with unknown or unclear functions have been discovered and classified into various groups depending on their half-life after transcription. The majority of ncRNAs are unstable (short-lived) as they are rapidly degraded by the RNA decay pathways. These include Cryptic Unstable Transcripts (CUTs) that were discovered in mutants of the nuclear exosome exonuclease component *RRP6* (Δ*rrp6*) (*9, 10*), Xrn1 exo-ribonuclease sensitive Unstable Transcripts (XUTs) (*2, 11*) and RNA-binding factor Nrd1 Unterminated Transcripts (NUTs) (*12*). There are also long-lived Stable Unannotated Transcripts (SUTs) that evade degradation in the nucleus and are processed in a similar manner to mRNA and exist in the wild type cell (*10*). The stability of SUTs implies that they are functional and involved in cellular processes. It is estimated that in the genome of *S. cerevisiae* there are >800 SUTs, >900 CUTs, >1800 XUTs and >1500 NUTs (*2, 10, 12*). These ncRNAs are transcribed from both sense and

antisense strands in relation to the coding genes from intra- and intergenic or open reading frame overlapping regions. Many of these ncRNAs overlap with each other and some are extended isoforms of other ncRNAs. Their molecular functions are still largely unknown.

Only a limited number of large-scale studies to identify the cellular functions ascribed to ncRNAs have been performed (*13-16*). Libraries of 1502 barcoded ncRNA deletion mutants in *S. cerevisiae* in both haploid (*MATa* and *MATα*) and diploid (homo- and heterozygote) backgrounds were constructed as tools for ncRNA functional analysis (*15, 17*). These libraries contain deletion mutants of tRNAs, snRNA, snoRNA, CUTs, SUTs and other annotated ncRNAs with a total number of 443 unique ncRNAs, that are localised to intergenic regions and do not overlap with protein coding genes, their promotors or terminators.

The yeast protein deletion collection has been successfully used to detect genetic interactions (GIs) and scored epistasis between protein coding genes by synthetic genetic array (SGA) screens (*18, 19*). Systematic mapping of genetic interaction was first automated in *S. cerevisiae* by employing the single open reading frame deletion collection composed of ~4800 genes crossed with 132 query strains using the SGA methodology (*20*). This approach led to identification of ~4000 genetic interactions between ~1000 protein coding genes and the construction of a large-scale genetic interaction map of the cell. Here, we employed the same methodology to shed light on the function of ncRNAs in *S. cerevisiae* by generating double ncRNA null mutants and analysing their genetic interactions by detecting double mutants with altered phenotypes. A ncRNA mutant library encompassing 378 ncRNAs was created in the SGA query strain Y7092 and an SGA study was conducted with a subset of 38 knock-out deletion mutants crossed with 411 previously generated single ncRNA deletion mutants (*15, 17*). The phenotypic effect of the double ncRNA deletions, compared to the single mutants, was then analysed in rich and non-fermentable media as well as in three stressor conditions, including oxidative, high temperature and osmotic stresses. The interactive network fitness data of the ncRNAs epistatic network has been deposited in the publicly accessible online resource, Yeast ncRNA Analysis (YNCA; http://sgjlab.org/ynca/). We discovered a total of 1003 epistatic interactions in rich media, of which ca. 10% were synthetic sick or lethal. Compared to the SGA protein-coding network, the ncRNAs mostly displayed positive interactions, and did not correlate with the epistasis of their neighbouring protein coding gene. We detected 395 “core” interactions shared in all condition tested and a significant number of environmental dependent interactions, including a differential SGA network for the two U3

snoRNA genes, SNR17A and SNR17B, suggesting a functional divergence of these two paralogs driven over time by different environmental pressures.

RESULTS AND DISCUSSION

Query ncRNA deletion mutant library construction and strain selection for SGA analysis

Single ncRNA deletion mutants in the Y7092 background (referred here as 'query') were generated by replacing the ncRNA of interest with the *natMX4* marker that confers nourseothricin resistance (clonNAT). A total number of 378 deletion mutant query strains were generated (Supplementary Dataset S1) and SGA analysis was conducted with 38 of them. Single mutant query strains with fitness defects are more likely to show a higher number of epistatic interactions compared to query strains with low or no fitness deficiency (*21*). In fact, there is a strong positive correlation between the number of genetic interaction and single-mutant fitness (r = 0.73) (*21*). Based on previous fitness studies (*15, 16*) that scored both the biomass (solid fitness of haploid ncRNA mutants) and the growth changes over time (competitive fitness of diploid heterozygous ncRNA deletion mutants), we chose 34 single ncRNA deletion strains which displayed either growth deficiency or haploinsufficiency under obligatory respiratory condition, high temperature, osmotic stress conditions, alternative carbon source such as sorbitol and melezitose or high concentration of ethanol (10%) and 4 strains with no significant fitness changes in any conditions (Supplementary Fig. 1).

SGA analysis of ncRNAs mutants reveals a prevalence of positive epistasis in the genetic interaction network

We performed SGA screens by crossing 38 query strains of interest with the ncRNA array library composed of 411 ncRNA deletion mutants (Supplementary Dataset S2), including 49 CUTs, 108 SUTs, 59 snoRNAs, 194 tRNAs and 1 unknown ncRNA RUF22. Approximately 6.4% (1003 interactions; Supplementary Dataset S3) of the 15,600 double mutant combinations generated, displayed either positive or negative significant epistasis (Fig. 1A). Positive epistasis was displayed by 905 (~90.2%) double mutants (Fig. 1B). In total, there were 98 (~9.8%) significant negative interactions of which 51 (~5.1%) and 47 (~4.7%) were synthetic sick (Fig. 1C) and synthetic lethal (Fig. 1D), respectively. Overall, each query ncRNAs had an average of 26 significant interactions, with numbers varying between 18 to 34 (Table 1, Supplementary Dataset S3).

Table 1: Number of significant SGA interactions between query and array strains, divided per ncRNA classes. The table shows the 1003 significant ncRNA-ncRNA interactions for 38 query strains analysed (fold change ≥2 and q-value ≤0.001) broken down according to type of ncRNAs. Positive and negative epistasis are represented with + and -, respectively. Refer to Supplementary Dataset S3 for detailed interactions.

	Number of interactions in the different ncRNA classes								Total interactions		
	CUTs		SUTs		SNRs		tRNAs		+	-	+ & -
Query	+	-	+	-	+	-	+	-			
CUT084-SUT068	4	0	9	1	0	1	10	2	23	4	27
CUT150	3	0	13	0	0	0	7	3	23	3	26
CUT244	1	0	8	1	0	1	6	7	15	9	24
SNR13	1	1	9	1	0	0	4	2	14	4	18
SNR17A	4	0	12	0	1	1	14	0	31	1	32
SNR17B	4	0	12	0	0	1	11	0	27	1	28
SNR34	3	0	10	0	0	0	12	2	25	2	27
SNR45	3	0	14	0	0	0	12	0	29	0	29
SNR71	3	0	12	0	1	0	11	0	27	0	27
SNR72	3	0	12	0	0	0	11	0	26	0	26
SNR72-78	3	0	12	0	0	0	11	2	26	2	28
SNR73	3	0	13	0	1	0	11	0	28	0	28
SNR74	3	0	12	0	1	0	11	0	27	0	27
SNR75	3	0	11	0	1	0	11	0	26	0	26
SNR76	2	0	11	0	0	0	10	0	23	0	23
SNR77	3	0	13	0	0	0	11	0	27	0	27
SNR78	3	0	13	0	1	0	11	0	28	0	28
SNR79	2	0	10	2	0	0	11	1	23	3	26
SNR8	3	0	13	0	0	0	11	1	27	1	28
SNR87	3	0	14	1	1	0	11	1	29	2	31
SUT083	3	0	13	0	0	0	12	0	28	0	28
SUT107	3	0	15	0	0	0	12	0	30	0	30
SUT193	3	2	7	2	0	1	9	2	19	7	26
SUT211	3	0	11	0	1	0	12	0	27	0	27
SUT289-SUT717	3	0	14	1	0	0	11	0	28	1	29
SUT361	0	1	9	0	0	0	8	2	17	3	20
SUT414	1	3	14	0	0	0	7	1	22	4	26
SUT420-CUT425	0	0	10	1	0	2	7	3	17	6	23
SUT457	3	1	13	0	1	0	11	0	28	1	29
SUT496	3	1	9	2	0	1	10	0	22	4	26
SUT532	1	3	6	2	0	3	9	3	16	11	27
SUT764	1	0	9	1	0	1	8	1	18	3	21
tD(GUC)M	2	0	13	1	0	0	9	1	24	2	26
tE(CUC)D	2	2	11	2	0	4	10	3	23	11	34
tE(UUC)M	1	1	9	2	0	1	9	0	19	4	23
tH(GUG)H	3	0	10	2	0	1	6	0	19	3	22
tI(AAU)N1	1	0	13	0	0	0	10	2	24	2	26
tV(AAC)G3	1	0	10	2	0	1	9	1	20	4	24
Total	91	15	429	24	9	19	376	40	905	98	1003

In contrast to protein-coding genes for which negative genetic interactions are approximately two-fold more prevalent than positive interactions (*21*), here a surprisingly large number of double mutants displayed positive epistasis, comprising ~90% of the significant interactions (Fig. 1A, Table 1). The prevalence of positive epistasis in the SGA network was also seen when interactions were broken down for each individual query strains. For example, SNR45, SNR71, SNR72, SNR73, SNR74, SNR75, SNR76, SNR77, SNR78, SUT083, SUT107 and SUT211 only displayed positive interactions (Table 1). The snoRNAs SNR72, SNR73, SNR74, SNR75, SNR76, SNR77 and SNR78 are in a tight cluster on the chromosome 13 and in the SGA are detected as synthetic lethal interactions because it is unlikely that any recombination is occurring between them. Such spurious inter-cluster interactions have been removed from our dataset. We also carried out SGA using the entire SNR72-78 cluster null mutant. In this case we detected two synthetic lethal interactions with two tRNAs on chromosome 2 and 12; both coding for leucine (Supplementary Dataset S3). Moreover, SNR66 (C/D box snoRNA) displayed 8 positive interactions, of which six were between snoRNAs (SNR71, SNR73, SNR74, SNR75, SNR78 and SNR87) and two with SUTs (SUT211 and SUT457) (Supplementary Dataset S3). Interestingly, SNR66 is involved in the same biochemical function (methylation of rRNAs) as SNR71, SNR73, SNR74, SNR75, SNR78 and SNR87. It has been reported previously that proteins that are part of the same complex and therefore physically interact with each other are threefold more likely to show positive epistasis (*18*). Hence, these snoRNA interactions may also reflect a physical relationship.

SUTs were responsible for the highest number of epistatic interactions, after normalisation for the total cohort (p-value $=1.66e^{-53}$), whereas snoRNAs displayed the least number of interactions (Table 1). These results are consistent with SUTs being transported to the cytoplasm similarly to mRNAs and acting as functional transcripts affecting important cellular functions (*16*, *22*, *23*).

The ncRNA genetic interaction networks, hosted in the Yeast NcRNA Analysis database (YNCA), can be explored as an interactive map through the link http://sgjlab.org:3838/ynca/, “interactive networks” tab.

Comparison between ncRNA and neighbouring protein interaction networks reveals poor overlap

To understand whether altered expression of genes flanking the ncRNAs indirectly influenced the ncRNA interaction network, we surveyed all genetic and physical interactions of the proteins encoded by the neighbouring genes, to determine the overlap between protein and ncRNA interaction networks. Intergenic ncRNAs could either work in *trans* and affect genes or transcription factors involved in cellular growth (*15, 16, 24*) or may provoke expressional changes in *cis* (*25-28*) and this expression change could cause the epistasis between the affected genes (*i.e.* synthetic interactions between the neighbouring genes due to expressional changes). Provided that the latter scenario is the most common, we should expect some overlap between the SGA network of ncRNAs and the SGA network of the neighbouring protein coding genes.

The BioGrid database was used to recover the interactions which are recorded as genetic or physical (*i.e.* protein-protein interactions scored either by affinity capture, protein-fragment complementation assay or two hybrid bait). We found that the overwhelming majority of the neighbouring genes (96.8%) flanking the ncRNAs involved in the ncRNA network had no recorded genetic or protein interactions (Fig. 2, and Supplementary Dataset S4). Recent data from transcriptome studies of ncRNA mutants revealed that the deletion of several SUTs has a global, rather than a local effect on gene transcription and can act on a large-scale by modulating expression of transcription factors (TFs) (*16*). For instance, in the absence of SUT532, SUT125 and SUT126 the expression of TFs that participate in the stress response, sporulation, cell cycle progression and cell integrity such as Xpb1, Rim1 Rgm1, Yox1, Rof1, Tos8, Msa1, and Tos4 was highly affected. Such modulation is scored as a growth advantage in the short term, although unlikely to render the cell fitter over time given that an accurate mitotic control is crucial to avoid multiple duplications and DNA damage.

Out of the 3.2% of ncRNAs which had neighbouring genes involved in interactions, ~64.5% were genetic and ~35.5% physical (Fig. 2). In this small subset most of the ncRNA genetic interactions were negative (21/24; 87.5%) leading to phenotypic suppression, synthetic growth defect and dosage lethality (Supplementary Dataset S4), mimicking the overall trend seen for the protein-coding gene network, where the majority of the interactions were negative(*29*). This neighbouring gene interaction suggests a potential *in cis* effect of the ncRNA on the flanking genes. Although when generating the ncRNA mutant collection (*15, 17*) every effort has been made to avoid deletion of either promotor or terminators of the adjacent protein coding genes,

it is possible that for some ncRNA double mutants the observed phenotype is due (or partially due) to altered expression of flanking genes.

The ncRNAs genetic interaction data can also reveal neighbouring gene epistasis from their overexpression (*i.e.* when altered expression of two genes together cause a phenotype but the altered expression of the single mutants does not). For example, upon SUT259/691 deletion, *EMP46* and *GAL4* are both overexpressed causing a lethal phenotype (*15*). Such epistatic interactions between proteins would not have been revealed by classical SGA analysis based on gene deletions.

Network dynamics of ncRNAs in different stress conditions reveal more negative epistatic interactions

Genetic epistasis is dependent on the genetic background and the environment(*30*) therefore, we analysed all single and double ncRNA mutants under five different nutritional and stress conditions (rich and non-fermentative media as well as oxidative, high temperature, and osmotic stresses) to detect environmental-specific deviation of growth and infer changes in the ncRNA network. We scored the fitness plasticity of the interaction networks with 31 query strains encompassing ~12,700 mutant combinations (Fig. 3, Table 2 and Supplementary Dataset S5). We observed that stress produces a significantly increased interactions, in particular negative interactions. High temperature stress (37°C) displayed more negative than positive epistatic interactions (Fig. 3B), an opposite trend than detected at 30°C (Fig. 3A). The highest number of interactions, either positive or negative, was observed under respiratory stress (YP+7% glycerol, 30°C; Fig. 3C) for which there were 40 times more negative interactions than in rich medium. Overall, the different stress conditions displayed at least two times more negative interactions than YPD at 30°C.

Interestingly, regardless of media and temperature, most interactions involving snoRNAs were positive. In fact, there are conditions where snoRNAs display no negative interactions. This result echoes the “monochromatic” nature observed in the protein-coding network, where genetic interactions between defined pathways tend to be either exclusively positive or exclusively negative (*21, 31*). Although the monochromatic effect is robust, the pattern of interactions between the functional modules could be considerably affected by environmental perturbations, as observed with a small number of snoRNA interactions when exposed to a particular stress condition (Fig. 4 and Supplementary Dataset S5).

Table 2: Number of significant ncRNA interactions after fitness profiling in different environmental conditions.

Condition	Total number of significant interactions	Number of positive interactions	Number of negative interactions
YPD, 30°C	839	716	123
YPD, 37°C	831	398	433
YP+7% glycerol, 30°C	1525	844	681
YPD+1 M NaCl, 30°C	1027	653	374
YPD+4 mM H_2O_2, 30°C	1145	734	411

Next, we identified ncRNA interactions that were shared and unique to each of the environmental conditions tested (absolute fold change ≥2 and q-value ≤0.001) (Fig. 4A, Supplementary Dataset S6). There were 395 "core" ncRNA interactions shared between all five conditions tested. One hundred and fifty-nine ncRNA interactions were specific only to rich medium (YPD, 30°C), 392 to glycerol (respiratory stress), 24 to NaCl (osmotic stress), 19 to 37°C (temperature stress) and 12 to hydrogen peroxide (oxidative stress). Interestingly, in all the four stress conditions tested 21% of the core interactions changed directionality compared to rich medium (Supplementary Fig. 2). Among those that changed, 5 negative interactions became positive and 79 positive interactions became negative, with exception for 7 interactions in osmotic shock medium (Fig. 4B). A visual representation of the plasticity of the interactions in different media conditions of selected single and double mutants is shown in Fig. 4C. The observed sub-networks with shared common ncRNAs that change directionality in the stress conditions suggests that these ncRNAs may have a primary function in stress response. For instance, we identify a prevalence of negative interactions under obligatory respiratory condition (YP+7% glycerol, 30°C) among ncRNAs that have previously described to display a pivotal role in cell fitness (*16*). In fact, SUT125, SUT126 and SUT035 share similar phenotypic and transcriptome changes under different environmental conditions (*16*). These ncRNAs, along with SUT532, appear to modulate genes *in trans* that are involved in mitochondrial functions. Remarkably, we identified 22 epistatic interactions in common among SUT125, SUT126, SUT035 with the presence of predominantly negative interactions under respiratory stress, YP+7% glycerol at 30°C (Fig. 4C, Supplementary Fig. 2 and Supplementary Dataset S3). In the same stress condition, SUT532 displayed 14 unique interactions with other ncRNAs (Supplementary Dataset S6).

The potential correlation between phenotypic changes in a single ncRNA deletion mutant and the number of SGA interactions was investigated using previously published fitness data (*15, 16*). We found that there is only a weak positive correlation between the fitness change of single mutants and the number of interactions (Supplementary Fig. 3 and Supplementary Dataset S5).

We also compared the ncRNA interactions in YPD and the other conditions with the available interaction network in minimal medium of the neighbouring protein coding genes. Again, only a small subset of neighbouring genes/proteins displayed interactions either genetic or physical (Supplementary Fig. 4 and Supplementary Dataset S7).

Analysis of the paralog snoRNAs, SNR17A and SNR17B

Next, we focused our attention on the yeast SNR17 (U3). In *S. cerevisiae* this snoRNA is transcribed from two genetic loci *SNR17A* and *SNR17B* located on separate chromosomes, XV and XVI, respectively. U3 is required for pre-rRNA processing, namely cleavage of 35S pre-rRNA leading to mature 18S rRNA production (*32, 33*). An early study suggested that these two paralogs may perform the same function in the cell since they share the same nuclear localisation and bind to 35S pre-rRNA (*34*). Our results reveal that deletion of SNR17B does not significantly change the phenotype compared to the WT, except in YP+7% glycerol, while the SNR17A deletion displays decreased growth in YPD 30°C, YPD 37°C and YPD+4 mM H_2O_2 (Supplementary Fig. 5). The double deletion of SNR17A and SNR17B is lethal (*34*) and our SGA results confirm it their lethality together.

The SGA network of SNR17A and SNR17B can help to understand whether the function of these two paralogs has diverged over evolutionary time. Thirty-one and 27 significant SGA interactions were detected in our screens in YPD at 30°C with SNR17AΔ and SNR17BΔ, respectively (Fig. 5A and Supplementary Dataset S8). As expected, the majority of interactions were shared between these two snoRNAs reflecting that they are functional homologs (Fig. 5a). In fact, only six interactions were unique to SNR17A and two to SNR17B in YPD 30°C and all displayed positive epistasis. However, surprisingly, a large increase in paralog specific interactions was observed in other environmental conditions (Fig. 5, B to E) and such specificity was not lost even using the most stringent q-value of 0.001 (Supplementary Fig. 6 and Supplementary Dataset S8). Interestingly, under obligatory respiration, oxidative, temperature and osmotic stresses, the interaction network exclusive to SNR17BΔ was highly

expanded, revealing 5 to 10 times more specific interactions than SNR17AΔ. This difference in the interaction network of SNR17A and SNR17B may indicate that since the duplication event, the paralogs have sub-functionalised, and SNR17B might also be modulating different cellular functions independently of its paralog SNR17A. Within the SNR17B specific network, seven interactions were in common in all stress conditions, five of which involving tRNAs. Interestingly, there is an overrepresentation of tRNAs in the specific network of SNR17B (p-value=0.05 Pearson's Chi-squared test, Yates' continuity correction) which suggest a potential role of SNR17B modulating/processing tRNAs. In other organisms, co-immunoprecipitation and high-throughput sequencing of ligated RNAs have revealed interactions between snoRNAs and other RNAs such as tRNA (*35*) and mRNAs (*36*). Moreover, snoRNAs have been reported to participate in methylation of tRNAs (*37*), regulating 3′ mRNA processing (*38*) and alternative splicing (*39*).

We tested the absolute expression of the two paralogs in three *S. cerevisiae* strains. Early studies to detect snoRNA levels in the cell by labelled probe hybridisation to total RNA revealed that SNR17A RNA was approximately 5 to 10-fold more abundant than SNR17B implicating SNR17A as the major player in 18S rRNA processing (*34, 40*). Contrary to these results, by using RT-qPCR, we observed that SNR17B RNA levels were three times higher than SNR17A in two haploid WT strains BY4741 and Y7092 (Fig. 6A). This difference in expression was also consistent when the snoRNA levels were measured in a natural diploid isolate, *S. cerevisiae* 96.2 (courtesy of E. Barrio) (*41*), suggesting that it is not strain dependent. For BY4741, we also tested the expression of the snoRNAs in presence of stressors (Fig. 6B). Here, except for YP-7% glycerol at 30°C, we observed again the same trend with SNR17B being the most highly expressed of the two paralogs. We also measured the expression of SNR17A and SNR17B in the mutants SNR17BΔ and SNR17AΔ, respectively. In the standard condition the levels of SNR17B were reduced almost to half when SNR17A was deleted, while levels of SNR17A displayed no significantly change in the SNR17BΔ deletion mutant (Fig. 6C). These data confirm that the rRNA processing function of SNR17A, with respect to SNR17B, is not due (or at least not only due) to its abundance, as previously suggested.

Deletion of SNR17A causes changes in 18S rRNA concentration

Since SNR17 is crucial for 35S pre-rRNA processing and maturation of 18S rRNA (*32, 33*), we hypothesised that the deletion of the U3 snoRNA paralogues would reduce the

concentration of the 18S rRNA fraction in the cell. We tested our hypothesis by measuring the concentration of 18S rRNA in the WT and deletion mutants grown in the yeast standard condition and four stressors (high temperature, obligatory respiration, oxidative and osmotic stresses) to determine if any 18S rRNA concentration changes are environmentally dependent.

Deletion of SNR17A resulted in a significant reduction of 18S rRNA fraction abundance when compared to the WT strain in four out of five conditions tested (Fig. 7A). This reduction in 18S rRNA concentration supports the established notion that SNR17A has a major role in pre-rRNA processing. However, no significant changes in 18S rRNA abundance were observed in the SNR17B deletion mutant, suggesting that SNR17B is not the key player in the maturation of 18S rRNA and may not mainly act as back up for SNR17A. Overall, these data suggest that SNR17B may have sub-functionalised and be involved in other cellular functions.

Since our SGA screens revealed a positive epistatic interaction between SNR17A and SUT480, most evident in the respiratory stress condition (Supplementary dataset S5), we investigated how the concentration of 18S rRNA is affected by the epistatic interaction of SNR17A and SUT480. We measured the concentration of 18S rRNA in both yeast standard condition and YP+7% glycerol at 30°C for the WT, single SNR17A and SUT480 deletion mutants and the double mutant SNR17AΔ/SUT480Δ (Fig. 7B). We found that the 18S rRNA concentration is decreased in both the single mutants SNR17AΔ and SUT480Δ. The reduction of 18S rRNA concentration in the single SUT480Δ mutant is more evident in the respiratory stress compared to the standard growth media. No additive decrease of 18S rRNA concentration was observed for the double mutant compared to single mutants. In fact, an increase in 18S concentration in glycerol was observed compared to the SUT480Δ. Such data validate the positive epistatic interaction detected in the SGA screen and suggest that these two ncRNAs synergistically affect rRNA processing through the same pathway. qPCR data reveals that SUT480, SNR17A and SNR17B do not affect each other's transcription levels in either of the lab strains tested (Supplementary Fig. 7, A to C). Moreover, deletion of SUT480 does not influence the expression of its neighbouring gene *RNH202*, which codes for the ribonuclease H2 subunit required for RNA hydrolysis when annealed to a complementary DNA (*42*) (Supplementary Fig. 7D), ruling out an indirect effect of the SUT480 phenotype acting by transcriptional interference.

CONCLUSIONS

This study constitutes a pioneering effort to determine the genetic interactions between 5 classes of ncRNAs, namely CUTs, SUTs, snoRNAs, tRNAs and RUF, and provides insights on their possible functions in yeast. We observed that the majority of genetic interactions between ncRNAs in the rich condition are positive (>~90%) as opposed to the predominantly negative genetic interactions scored for the protein network (*18*). This positive epistasis indicates that most of the ncRNA have presumably repressive regulatory functions in the cell. The networks of ncRNAs and their neighbouring genes are primarily independent, showing little overlap between each other. The small subsets of genetic networks that do overlap are composed predominantly by negative interactions, suggesting a potential effect *in cis* of the ncRNA on the flanking genes.

The environment has a significant impact on the ncRNA genetic interaction network. We observed an increase in the number of negative interactions in all stress conditions tested, with the highest number recorded in glycerol (up to 40 times more compared to rich media). This result suggests that these ncRNAs have unique functions in the cell or are being differentially transcribed depending on the environment.

The interaction data acquired in this study is also useful for teasing apart cellular roles of ncRNA duplicates and to find whether their functions have diverged over evolutionary time, as in the case of snoRNAs SNR17A and SNR17B. By measuring the expression of SNR17A and SNR17B in the cell and the concentration of 18S rRNA in SNR17A and SNR17B mutants, we confirmed that SNR17A is a major player in rRNA processing and this function is not because of SNR17A abundance. Looking at SNR17A and SNR17B genetic networks in rich medium, the two paralogues share the majority of genetic interactions, as expected. However, under stress conditions, SNR17B displayed a large number of unique epistatic interactions suggesting that they may have sub-functionalised as result of functional divergence that occurs after genome duplication (*43, 44*), and has acquired other roles in the cell. We found that SUT480 is genetically interacting with SNR17A, we linked its function to the processing of 18S rRNA, and validated the scored epistasis.

Overall, this study offers the first insight in the environmentally-dependent epistatic interactions of ncRNAs in an eukaryotic organism.

MATERIALS AND METHODS

Strains and plasmids

We previously generated a library of ncRNA mutants in both haploid and diploid backgrounds (*15, 17*). The *MAT***a** library from this collection (Supplementary Dataset S2), referred here as 'array', was used in the crossing with the haploid *MATα* 'query' single deletion strains (generated in this study; Supplementary Dataset S1) to create double mutant according to the SGA protocol (*18*). The *MAT***a** array library was constructed in the BY4741 background (*his3Δ1 leu2Δ0 met15Δ0 ura3Δ0*) and all these mutants carry a *kanMX* resistance gene that replaced the ncRNAs of interest (*17*). The *MATα* query collection was generated in the Y7092 background (*can1Δ::STE2pr-Sp_his5 lyp1Δ ura3Δ0 leu2Δ0 his3Δ1 met15Δ0*; kindly provided by the Boone lab) (*18*). The query ncRNA deletion strains carry the *natMX4* resistance marker that replaced the ncRNAs of interest. This *natMX4* marker confers clonNAT (Nourseothricin; WERNER BioAgents GmbH) antibiotic resistance and was amplified from the pFA6-*natMX4* (*45*) plasmid in a single PCR step using primers partly complementary to the ncRNA flanking sequences. A natural diploid *S. cerevisiae* strain 96.2 (*41*) was used to test differential expression of SNR17A and SNR17B.

Query strain library construction

The query strains were constructed by substituting the ncRNA loci with the *natMX4* cassettes. Each cassette was amplified using a pair of barcoded primers containing genome complementary sequences (*46*) from pFA6-*natMX4* in the total of 25 µl PCR volume: 10 ng plasmid DNA, 5 µM of forward and 5 µM of reverse primers, 10 mM of each dNTP, 2.5 units of LongAmp polymerase (New England Biolabs) and 1x of reaction buffer. The cycling conditions were as follows: initial denaturation at 95°C for 2 min followed by 35 cycles of 94°C for 30 sec, 58°C for 30 sec and 65°C for 1.5 min and 1 step of final elongation of 65°C for 5 min. The amplified PCR products were ~1.5 kb and they were transformed into the Y7092 (*MATα*) background strain. Transformants were selected on YPD agar (1% yeast extract, 2% peptone, 2% dextrose, 2% agar) supplemented with 200 µg/ml of clonNAT (Werner BioAgents, Jena, Germany). After 4 days of growth at 30°C, 1 to 5 colonies were streaked and single colonies were confirmed by colony PCR for correct cassette integration. The list of all query strains constructed in this study can be found in Supplementary Dataset S1.

PCR confirmation of query strains

Correct ncRNA locus deletion was confirmed by colony PCR. Following transformation, streaked colonies were resuspended in 100 µl sterile H_2O. Three sets of primers were used: (i) confA-confNatR, (ii) confNatF-confD and (iii) confA-confB (Supplementary Fig. 8, Supplementary Table S1). Confirmation primers confA, confB and confD are listed in Parker *et al*., 2017 (*17*). Primer pairs (i) and (ii) only generated PCR products if the ncRNA was replaced with the deletion cassette. Primer set (iii) generated PCR products if the ncRNA was intact and these colonies were discarded. The PCR was performed in the total volume of 25 µl and contained 5 µl of resuspended cells, 5 µM of forward and 5 µM of reverse primers, 10 mM of each dNTP, 2.5 units of LongAmp and 1x of reaction buffer. The same PCR conditions as above were used, generating PCR products between 0.6 kb and 1.2 kb, depending on the deleted ncRNA, which were analysed on a 1.5% agarose gel. Confirmed colonies were stored in YPD containing 15% glycerol at -80C until needed.

Single deletion ncRNA library formatting for SGA

The single deletion array library (*MATa*; ncRNA*::kanMX4*) is composed of 411 mutants encompassing 49 CUTs, 108 SUTs, 59 snoRNAs, 194 tRNAs and 1 RUF (Supplementary Dataset S2) (*17*). The library was first organised in 96 and 384 density formats and subsequently used as a source to generate the final working copy of two Plus Plates (Singer Instruments, UK) in a density of 1536 colonies per plate using the RoToR HDA system (Singer Instruments, UK). Each single deletion strain was plated in quadruplicates allowing replicates for consistent SGA analysis. The edges of each plate were excluded from the SGA analyses since colonies that are located on the edges and corners have more nutrient availability and decreased competition with the neighbouring colonies and hence often show increased growth (*47*). To minimise contamination, the single deletion ncRNA plates were grown on YPD agar supplemented with 200 µg/ml G418 (Sigma-Aldrich) or SD complete amino acid agar (0.67% yeast nitrogen base with amino acids (Merck), 2% glucose, 2% agar) supplemented with 200 µg/ml G418. The images of these plates were recorded using a Phenobooth (Singer Instruments) for subsequent SGA analyses.

Generation of the double ncRNA mutants using SGA

Thirty-eight query ncRNA deletion mutant strains (*MATα*; ncRNA*::natMX4*) (Supplementary Dataset S1) were selected to generate a library of double ncRNA deletion mutants. Prior to SGA, a small portion of -80°C cell cultures of these query strains was grown overnight in 5 ml

of liquid YPD at 30°C with shaking (200 rpm). Subsequently, 1 ml of the overnight cultures was spread onto PlusPlates containing YPD supplemented with 200 µg/ml of clonNAT using plastic cell spreaders and grown overnight at 30°C. Then, the query strains were crossed with the array ncRNA deletion library in the 1536 format on YPD agar using a RoToR HDA robot and disposable plastic replicators (pinning RePads, Singer Instruments, UK). SGA was carried out according to Baryshnikova, *et al.*, 2010 (*18*) including the generation of the double ncRNAs mutants library and subsequent analysis of epistasis.

Quality control of the double mutants created using SGA

Following SGA, 20 randomly selected haploid ncRNA double mutants were validated by PCR. The following primer sets were used for ncRNA1::*kanMX4* validation: (i) confA+confKanR, (ii) confD+confKanF and (iii) confA+confB. Primer sets (i) confA+confNatR, (ii) confD+confNatF and (iii) confA+confB were used for ncRNA2::*natMX4* validation in the same mutant (Supplementary Fig. 9, Supplementary Table S1).

SGA data analysis

Following SGA, images of the final selection plates containing generated double ncRNA mutants were recorded in white light using a Phenobooth and cropped using Corel PaintShop Pro X7. Subsequently, the images were processed using the high-throughput SGA data analysis software *Balony* (*48*) that measures colony area in pixels. The initial normalisation was performed in this software to correct for uneven plate growth according to the plate median and the row/column correction was applied. Minimum and maximum spot sizes were set to 0.02 and 100, respectively. Following the initial image processing in the *Balony* software, generated data was analysed using the R package version 3.4.4 (*49*). Recorded output size values for single and double mutant colonies were used to generate SGA scores using a script available on the SGATools website (http://sgatools.ccbr.utoronto.ca/) as well as in Baryshnikova, *et al.* (*18*) and Wagih *et al.* (*50*)) colonies on the periphery of the plates (as described above), (ii) single and double ncRNA mutants that showed inconsistent growth patterns among the quadruplicates and (iii) linkage group of ncRNAs that were on the same chromosome and were scored as lethal after the SGA as their phenotype was likely to be linked to the lack of meiotic crossing-over between them. The data was processed using an in-house R script. Assuming a normal distribution, p-values were calculated for each sample mean using the Z-score. The Z-score was found by assuming that the null hypothesis was true, subtracting the assumed mean, and dividing by the theoretical standard deviation. Q-values, which are

Bonferroni-adjusted p-values, were inferred using the "stats" R package (*49*). Absolute fold change ≥2 and q-value ≤0.001 thresholds were applied to select most significant interactions. The "UpSetR" R and "matplotlib_venn" python packages were used for data visualisation. The R pipeline created for this analysis is available at https://github.com/Sookie-S/SGA-analysis.

SGA network generation

Genomic interaction networks were created from the data generated for all experimental conditions tested. These included yeasts grown in rich media as well as on non-fermentable media, oxidative, high temperature and osmotic stress environments. The networks were generated using the "visNetwork" and "igraph" R libraries (*51, 52*). Nodes represent the ncRNAs and the edges represent the genetic interaction between them. The size of the nodes is proportional to the number of connections with the other nodes. The edges are coloured in green and red to distinguish the positive and negative epistasis, respectively. The thickness of the edges is proportional to the absolute value of fold change. The force-directed layout (forceAtlas2Based solver) (*53*) has been used to organize the graph in a 2D space. The central gravity of the networks is distance independent. The repulsion between the nodes is linear.

Phenotypic analysis of the mutants in stress conditions

The phenotypic analysis of both double and single deletion strains was performed in five different environmental conditions on solid growth media. These included (i) yeast rich media, YPD agar at 30°C, and four stress conditions: (ii) high temperature on YPD agar at 37°C, (iii) obligatory respiratory on YP agar supplemented with 7% glycerol at 30°C, (iv) osmotic stress on YPD agar supplemented with 1 M NaCl at 30°C and (v) oxidative stress on YPD agar supplemented with 4 mM H_2O_2 at 30°C. The single and double deletion library was analysed in the same 1536 format as described for SGA above. All cells were first grown on solid YPD agar media for 48h prior to the experiment and subsequently transferred on the specific experimental plates using the RoToR HDA system and grown for 48h at their relevant temperatures before analyses. The images of these plates were recorded using a Phenobooth and analysed using the *Balony* software in the similar manner as described for the SGA above. We used the same cut-off analysis values (absolute fold change ≥2 and q-value ≤0.001) as described above for the SGA analysis in standard yeast condition.

Genetic and physical interactions between neighbouring genes/proteins of interacting ncRNAs

Protein-protein physical interactions as well as genetic interactions between coding genes that were located in the neighbourhood of every interacting ncRNA pairs were analysed. Only significantly interacting ncRNA pairs were included (with absolute fold change ≥2 and q-value ≤0.001). A synthetic genome annotation file (BED file format) containing the names of protein coding genes and ncRNAs, their positions and strand information, was generated using an in-house Python 3.6 script. Gene annotations were extracted from the *Saccharomyces* genome database (SGD; www.yeastgenome.org/) and ncRNA annotations were added manually based on the information from Wery *et al*., 2016 (*2*). Subsequently, the genes and ncRNA were ordered by their start position and by the chromosome number using the BedTools sort tool (*54*). The flanking genes for each ncRNA were extracted using an in-house Python 3.6 script, generating 4 combinations of gene interactions for each pair of interacting double ncRNAs. A Python 3.6 script that uses the Representational State Transfer (REST) Application Programming Interface (API) of BioGRID database (https://thebiogrid.org/) was developed to query and access its data on the protein coding gene interaction data (physical and genetic) as well as phenotype observed and experiment type (https://github.com/Sookie-S/SGA-analysis).

Growth analysis of SNR17AΔ and SNR17BΔ mutants

A spot growth assay was performed on the single SNR17AΔ and SNR17BΔ mutants in the yeast standard media to reveal phenotypic effects of the snoRNA deletion. Three biological replicates were tested for each mutant. The growth was compared to the host strain Y7092. Cells for the spot assay were prepared in the following way: cells were grown overnight with shaking (200 rpm) and the cultures were centrifuged for 2 min at 2000 rpm. The pellet was resuspended in YPD and diluted to a starting OD_{600} of 1.0. Two and ten times dilutions were prepared and 1 and 5 µl of the cell suspensions was spotted on an agar plate which was incubated for 48h at 30°C or 37°C depending on the environmental condition. The growth was recorded every 12h of incubation.

SNR17AΔ and SNR17BΔ RNA extraction and RT-qPCR

Total RNA was extracted in the logarithmic growth phase using the RNeasy RNA isolation kit (Qiagen). Synthesis of complementary DNA was performed using QuantiTect Reverse Transcription Kit (Qiagen) following the manufacturer's instructions. Analysis of gene expression was performed using a The LightCycler® 480 real-time PCR System (Roche). The

gene *ACT1* was used as endogenous control. The Ct values obtained from three independent biological replicates were used to calculate the relative gene expression of the target genes according to the ΔΔCt method described by Livak and Schmittgen, 2001 (*55*). Statistical tests were performed using Welch two sample t-test and multiple comparisons were analysed using ANOVA followed by Dunnett's test or Tukey-Kramer test, according to the experiment. Error bars denote standard deviations; * $p < 0.05$; ** $p < 0.01$; *** $p < 0.001$; **** $p < 0.0001$; ns = no significant change. The RT-qPCR primers are listed in Supplementary Table S1. The SNR17A and SNR17B primers were designed to span the intron and their specificity were verified by RT-qPCR.

Quantitative analysis of 18S rRNA processing in ncRNA deletion mutants

The concentration of processed 18S rRNA in the wild-type (WT) as well as in the single ncRNA SNR17AΔ and SNR17BΔ mutants was performed in 5 different growth conditions. Additionally, we analysed the 18S concentrations in the WT and SNR17AΔ, SUT480Δ, SNR17A/SUT480Δ in the yeast standard growth condition and the respiratory stress. Total RNA was extracted in the logarithmic growth phase as described above and the RNA was processed using an RNA ScreenTape kit following the manufacturer's instructions. The RNA samples were run on a TapeStation 2200 system (Agilent Technologies). The error bars were calculated using the results from six technical replicates, and the p-values were determined using Welch's *t*-test.

ACKNOWLEDGMENTS

This work was supported by the Wellcome Trust, under the grant number 094225 to RTO and DD and 104981 to RTO, SGJ and DD. ST is supported by the European Research Council, H2020-MSCA-ITN-2017, under the grant number 764364 awarded to DD (https://cordis.europa.eu/project/id/764364). LNB was supported by The National Secretary of Higher Education, Science, Technology and Innovation (SENESCYT, http://siau.senescyt.gob.ec/), Ecuador and is currently funded by the Biotechnology and Biological Sciences Research Council (BB/T002123/1) to DD. KD scholarship was funded by the Royal Government of Thailand under the scheme for Development and Promotion of Science and Technology Talent (DPST) projects. MWF was supported by The University of Manchester - China Scholarship Council joint scholarship. The authors wish to thank Charlie Boone, Michael Costanzo and Sondra Bahr for useful discussions, provision of the Y7092

strain and help with the SGA methodology. The authors also thank Diego Estrada-Rivadeneyra for initial help with U3 snoRNA data acquisition.

DATA AVAILABILITY

The interactive network fitness data of the ncRNAs epistatic network has been added to the publicly accessible online resource, the Yeast ncRNA Analysis (YNCA) available here: http://sgjlab.org/ynca/

CODE AVAILABILITY

Codes used to analyse the data in this manuscript are available at https://github.com/Sookie-S/SGA-analysis.

REFERENCES

1. T. H. Jensen, A. Jacquier, D. Libri, Dealing with pervasive transcription. *Mol Cell* **52**, 473-484 (2013).
2. M. Wery, M. Descrimes, N. Vogt, A. S. Dallongeville, D. Gautheret, A. Morillon, Nonsense-Mediated Decay Restricts LncRNA Levels in Yeast Unless Blocked by Double-Stranded RNA Structure. *Mol Cell* **61**, 379-392 (2016).
3. J. Wu, D. Delneri, R. T. O'Keefe, Non-coding RNAs in Saccharomyces cerevisiae: what is the function? *Biochem Soc Trans* **40**, 907-911 (2012).
4. R. Boland, Non-coding RNA: It's Not Junk. *Dig Dis Sci* **62**, 1107-1109 (2017).
5. R. A. de Almeida, M. G. Fraczek, S. Parker, D. Delneri, R. T. O'Keefe, Non-coding RNAs and disease: the classical ncRNAs make a comeback. *Biochem Soc Trans* **44**, 1073-1078 (2016).
6. U. Nagalakshmi, Z. Wang, K. Waern, C. Shou, D. Raha, M. Gerstein, M. Snyder, The transcriptional landscape of the yeast genome defined by RNA sequencing. *Science* **320**, 1344-1349 (2008).
7. I. A. Drinnenberg, D. E. Weinberg, K. T. Xie, J. P. Mower, K. H. Wolfe, G. R. Fink, D. P. Bartel, RNAi in budding yeast. *Science* **326**, 544-550 (2009).
8. S. A. Shabalina, E. V. Koonin, Origins and evolution of eukaryotic RNA interference. *Trends Ecol Evol* **23**, 578-587 (2008).
9. H. Neil, C. Malabat, Y. d'Aubenton-Carafa, Z. Xu, L. M. Steinmetz, A. Jacquier, Widespread bidirectional promoters are the major source of cryptic transcripts in yeast. *Nature* **457**, 1038-1042 (2009).
10. Z. Xu, W. Wei, J. Gagneur, F. Perocchi, S. Clauder-Munster, J. Camblong, E. Guffanti, F. Stutz, W. Huber, L. M. Steinmetz, Bidirectional promoters generate pervasive transcription in yeast. *Nature* **457**, 1033-1037 (2009).
11. E. L. van Dijk, C. L. Chen, Y. d'Aubenton-Carafa, S. Gourvennec, M. Kwapisz, V. Roche, C. Bertrand, M. Silvain, P. Legoix-Ne, S. Loeillet, A. Nicolas, C. Thermes, A. Morillon, XUTs are a class of Xrn1-sensitive antisense regulatory non-coding RNA in yeast. *Nature* **475**, 114-117 (2011).
12. D. Schulz, B. Schwalb, A. Kiesel, C. Baejen, P. Torkler, J. Gagneur, J. Soeding, P. Cramer, Transcriptome surveillance by selective termination of noncoding RNA synthesis. *Cell* **155**, 1075-1087 (2013).

13. Z. Bloom-Ackermann, S. Navon, H. Gingold, R. Towers, Y. Pilpel, O. Dahan, A comprehensive tRNA deletion library unravels the genetic architecture of the tRNA pool. *PLoS Genet* **10**, e1004084 (2014).
14. F. Huber, D. Bunina, I. Gupta, A. Khmelinskii, M. Meurer, P. Theer, L. M. Steinmetz, M. Knop, Protein Abundance Control by Non-coding Antisense Transcription. *Cell Rep* **15**, 2625-2636 (2016).
15. S. Parker, M. G. Fraczek, J. Wu, S. Shamsah, A. Manousaki, K. Dungrattanalert, R. A. de Almeida, E. Invernizzi, T. Burgis, W. Omara, S. Griffiths-Jones, D. Delneri, R. T. O'Keefe, Large-scale profiling of noncoding RNA function in yeast. *PLoS Genet* **14**, e1007253 (2018).
16. L. N. Balarezo-Cisneros, S. Parker, M. G. Fraczek, S. Timouma, P. Wang, R. T. O'Keefe, C. B. Millar, D. Delneri, Functional and transcriptional profiling of non-coding RNAs in yeast reveal context-dependent phenotypes and in trans effects on the protein regulatory network. *PLoS Genet* **17**, e1008761 (2021).
17. S. Parker, M. G. Fraczek, J. Wu, S. Shamsah, A. Manousaki, K. Dungrattanalert, R. A. de Almeida, D. Estrada-Rivadeneyra, W. Omara, D. Delneri, R. T. O'Keefe, A resource for functional profiling of noncoding RNA in the yeast Saccharomyces cerevisiae. *RNA* **23**, 1166-1171 (2017).
18. A. Baryshnikova, M. Costanzo, S. Dixon, F. J. Vizeacoumar, C. L. Myers, B. Andrews, C. Boone, Synthetic genetic array (SGA) analysis in Saccharomyces cerevisiae and Schizosaccharomyces pombe. *Methods Enzymol* **470**, 145-179 (2010a).
19. A. H. Tong, C. Boone, Synthetic genetic array analysis in Saccharomyces cerevisiae. *Methods Mol Biol* **313**, 171-192 (2006).
20. A. H. Tong, G. Lesage, G. D. Bader, H. Ding, H. Xu, X. Xin, J. Young, G. F. Berriz, R. L. Brost, M. Chang, Y. Chen, X. Cheng, G. Chua, H. Friesen, D. S. Goldberg, J. Haynes, C. Humphries, G. He, S. Hussein, L. Ke, N. Krogan, Z. Li, J. N. Levinson, H. Lu, P. Menard, C. Munyana, A. B. Parsons, O. Ryan, R. Tonikian, T. Roberts, A. M. Sdicu, J. Shapiro, B. Sheikh, B. Suter, S. L. Wong, L. V. Zhang, H. Zhu, C. G. Burd, S. Munro, C. Sander, J. Rine, J. Greenblatt, M. Peter, A. Bretscher, G. Bell, F. P. Roth, G. W. Brown, B. Andrews, H. Bussey, C. Boone, Global mapping of the yeast genetic interaction network. *Science* **303**, 808-813 (2004).
21. M. Costanzo, A. Baryshnikova, J. Bellay, Y. Kim, E. D. Spear, C. S. Sevier, H. Ding, J. L. Koh, K. Toufighi, S. Mostafavi, J. Prinz, R. P. St Onge, B. VanderSluis, T. Makhnevych, F. J. Vizeacoumar, S. Alizadeh, S. Bahr, R. L. Brost, Y. Chen, M. Cokol, R. Deshpande, Z. Li, Z. Y. Lin, W. Liang, M. Marback, J. Paw, B. J. San Luis, E. Shuteriqi, A. H. Tong, N. van Dyk, I. M. Wallace, J. A. Whitney, M. T. Weirauch, G. Zhong, H. Zhu, W. A. Houry, M. Brudno, S. Ragibizadeh, B. Papp, C. Pal, F. P. Roth, G. Giaever, C. Nislow, O. G. Troyanskaya, H. Bussey, G. D. Bader, A. C. Gingras, Q. D. Morris, P. M. Kim, C. A. Kaiser, C. L. Myers, B. J. Andrews, C. Boone, The genetic landscape of a cell. *Science* **327**, 425-431 (2010).
22. D. Kyriakou, E. Stavrou, P. Demosthenous, G. Angelidou, B. J. San Luis, C. Boone, V. J. Promponas, A. Kirmizis, Functional characterisation of long intergenic non-coding RNAs through genetic interaction profiling in Saccharomyces cerevisiae. *BMC Biol* **14**, 106 (2016).
23. A. C. Tuck, D. Tollervey, A transcriptome-wide atlas of RNP composition reveals diverse classes of mRNAs and lncRNAs. *Cell* **154**, 996-1009 (2013).
24. J. Camblong, N. Beyrouthy, E. Guffanti, G. Schlaepfer, L. M. Steinmetz, F. Stutz, Trans-acting antisense RNAs mediate transcriptional gene cosuppression in S. cerevisiae. *Genes Dev* **23**, 1534-1545 (2009).
25. J. A. Martens, L. Laprade, F. Winston, Intergenic transcription is required to repress the Saccharomyces cerevisiae SER3 gene. *Nature* **429**, 571-574 (2004).
26. J. Camblong, N. Iglesias, C. Fickentscher, G. Dieppois, F. Stutz, Antisense RNA stabilization induces transcriptional gene silencing via histone deacetylation in S. cerevisiae. *Cell* **131**, 706-717 (2007).

27. P. Thebault, G. Boutin, W. Bhat, A. Rufiange, J. Martens, A. Nourani, Transcription regulation by the noncoding RNA SRG1 requires Spt2-dependent chromatin deposition in the wake of RNA polymerase II. *Mol Cell Biol* **31**, 1288-1300 (2011).
28. F. J. van Werven, G. Neuert, N. Hendrick, A. Lardenois, S. Buratowski, A. van Oudenaarden, M. Primig, A. Amon, Transcription of two long noncoding RNAs mediates mating-type control of gametogenesis in budding yeast. *Cell* **150**, 1170-1181 (2012).
29. M. Usaj, Y. Tan, W. Wang, B. VanderSluis, A. Zou, C. L. Myers, M. Costanzo, B. Andrews, C. Boone, TheCellMap.org: A Web-Accessible Database for Visualizing and Mining the Global Yeast Genetic Interaction Network. *G3 (Bethesda)* **7**, 1539-1549 (2017).
30. J. van Leeuwen, C. Pons, J. C. Mellor, T. N. Yamaguchi, H. Friesen, J. Koschwanez, M. M. Usaj, M. Pechlaner, M. Takar, M. Usaj, B. VanderSluis, K. Andrusiak, P. Bansal, A. Baryshnikova, C. E. Boone, J. Cao, A. Cote, M. Gebbia, G. Horecka, I. Horecka, E. Kuzmin, N. Legro, W. Liang, N. van Lieshout, M. McNee, B. J. San Luis, F. Shaeri, E. Shuteriqi, S. Sun, L. Yang, J. Y. Youn, M. Yuen, M. Costanzo, A. C. Gingras, P. Aloy, C. Oostenbrink, A. Murray, T. R. Graham, C. L. Myers, B. J. Andrews, F. P. Roth, C. Boone, Exploring genetic suppression interactions on a global scale. *Science* **354**, (2016).
31. D. Segre, A. Deluna, G. M. Church, R. Kishony, Modular epistasis in yeast metabolism. *Nat Genet* **37**, 77-83 (2005).
32. E. S. Maxwell, M. J. Fournier, The small nucleolar RNAs. *Annu Rev Biochem* **64**, 897-934 (1995).
33. J. L. Woolford, Jr., S. J. Baserga, Ribosome biogenesis in the yeast Saccharomyces cerevisiae. *Genetics* **195**, 643-681 (2013).
34. J. M. Hughes, D. A. Konings, G. Cesareni, The yeast homologue of U3 snRNA. *EMBO J* **6**, 2145-2155 (1987).
35. A. M. Kiss, B. E. Jady, E. Bertrand, T. Kiss, Human box H/ACA pseudouridylation guide RNA machinery. *Mol Cell Biol* **24**, 5797-5807 (2004).
36. E. Sharma, T. Sterne-Weiler, D. O'Hanlon, B. J. Blencowe, Global Mapping of Human RNA-RNA Interactions. *Mol Cell* **62**, 618-626 (2016).
37. P. Vitali, T. Kiss, Cooperative 2'-O-methylation of the wobble cytidine of human elongator tRNA(Met)(CAT) by a nucleolar and a Cajal body-specific box C/D RNP. *Genes Dev* **33**, 741-746 (2019).
38. C. Huang, J. Shi, Y. Guo, W. Huang, S. Huang, S. Ming, X. Wu, R. Zhang, J. Ding, W. Zhao, J. Jia, X. Huang, A. P. Xiang, Y. Shi, C. Yao, A snoRNA modulates mRNA 3' end processing and regulates the expression of a subset of mRNAs. *Nucleic Acids Res* **45**, 8647-8660 (2017).
39. S. Kishore, S. Stamm, The snoRNA HBII-52 regulates alternative splicing of the serotonin receptor 2C. *Science* **311**, 230-232 (2006).
40. E. Myslinski, V. Segault, C. Branlant, An intron in the genes for U3 small nucleolar RNAs of the yeast Saccharomyces cerevisiae. *Science* **247**, 1213-1216 (1990).
41. C. M. Paget, J. M. Schwartz, D. Delneri, Environmental systems biology of cold-tolerant phenotype in Saccharomyces species adapted to grow at different temperatures. *Mol Ecol* **23**, 5241-5257 (2014).
42. H. S. Jeong, P. S. Backlund, H. C. Chen, A. A. Karavanov, R. J. Crouch, RNase H2 of Saccharomyces cerevisiae is a complex of three proteins. *Nucleic Acids Res* **32**, 407-414 (2004).
43. A. Force, M. Lynch, F. B. Pickett, A. Amores, Y. L. Yan, J. Postlethwait, Preservation of duplicate genes by complementary, degenerative mutations. *Genetics* **151**, 1531-1545 (1999).
44. A. Stoltzfus, On the possibility of constructive neutral evolution. *J Mol Evol* **49**, 169-181 (1999).
45. A. Wach, A. Brachat, R. Pohlmann, P. Philippsen, New heterologous modules for classical or PCR-based gene disruptions in Saccharomyces cerevisiae. *Yeast* **10**, 1793-1808 (1994).
46. A. M. Chu, R. W. Davis, High-throughput creation of a whole-genome collection of yeast knockout strains. *Methods Mol Biol* **416**, 205-220 (2008).
47. A. Baryshnikova, M. Costanzo, Y. Kim, H. Ding, J. Koh, K. Toufighi, J. Y. Youn, J. Ou, B. J. San Luis, S. Bandyopadhyay, M. Hibbs, D. Hess, A. C. Gingras, G. D. Bader, O. G. Troyanskaya, G.

W. Brown, B. Andrews, C. Boone, C. L. Myers, Quantitative analysis of fitness and genetic interactions in yeast on a genome scale. *Nat Methods* **7**, 1017-1024 (2010b).

48. B. P. Young, C. J. Loewen, Balony: a software package for analysis of data generated by synthetic genetic array experiments. *BMC Bioinformatics* **14**, 354 (2013).
49. R. C. team. (2021).
50. O. Wagih, M. Usaj, A. Baryshnikova, B. VanderSluis, E. Kuzmin, M. Costanzo, C. L. Myers, B. J. Andrews, C. M. Boone, L. Parts, SGAtools: one-stop analysis and visualization of array-based genetic interaction screens. *Nucleic Acids Res* **41**, W591-596 (2013).
51. B. T. a. T. R. Almende B.V. and Contributors. (2021).
52. N. T. Csardi G, The igraph software package for complex network research, InterJournal, Complex Systems 1695. 2006. (2006).
53. M. Jacomy, T. Venturini, S. Heymann, M. Bastian, ForceAtlas2, a continuous graph layout algorithm for handy network visualization designed for the Gephi software. *PLoS One* **9**, e98679 (2014).
54. A. R. Quinlan, I. M. Hall, BEDTools: a flexible suite of utilities for comparing genomic features. *Bioinformatics* **26**, 841-842 (2010).
55. K. J. Livak, T. D. Schmittgen, Analysis of relative gene expression data using real-time quantitative PCR and the 2(-Delta Delta C(T)) Method. *Methods* **25**, 402-408 (2001).

FIGURE LEGENDS

FIG. 1. ncRNA SGA network for 38 query strains. The SGA network was generated based on the absolute fold change ≥2 and q-value ≤0.001 cut off for 38 query ncRNA deletion strains. The nodes are coloured by class of ncRNA. Orange: SUTs; red: CUTs; purple: snoRNAs; green: tRNAs. (**A**) Total epistatic interaction network between ncRNAs. (**B**) Positive interactions between ncRNA deletions. (**C**) Negative synthetic sick interactions. (**D**) Negative synthetic lethal interactions. The node size is proportional to the number of interactions they are involved in. Black and grey edges represent negative and positive epistasis, respectively. The thickness of the edges is proportional to the strength of the interaction.

FIG. 2. Analysis of the interactions of genes neighbouring epistatic pairs of ncRNAs. (**A**) Strategy to analyse genetic and physical interactions between the neighbouring protein coding genes (green arrows) of ncRNA pairs showing significant epistasis (orange). (**B**) Pie charts displaying the proportion of significantly interacting neighbouring genes (dark blue colour), broken down in genetic (mid blue) and physical interactions (light blue).

FIG. 3. Visualization of the ncRNA network under different environmental condition. ncRNA network generated for 31 query ncRNA deletion strains based on the absolute fold change ≥2 and q–value ≤0.001 cut off in (**A**) YPD, 30°C, (**B**) YPD, 37°C, (**C**) YP+7% Glycerol, 30°C, (**D**) YPD+1 M NaCl, 30°C and (**E**) YPD+4 mM H_2O_2, 30°C. Network ncRNAs nodes (blue); red edges – negative ncRNA genetic interactions, green edges – positive ncRNA genetic interactions. The thickness of the edges is proportional to the absolute fold change.

FIG. 4. Environmental conditions elicit yeast ncRNA interaction network changes. (**A**) Upset plot depicting environmental unique and shared ncRNA genetic interactions between the five conditions tested (YPD, 37°C; YPD, 30°C; YPD+1 M NaCl, 30°C; YPD+4 mM H_2O_2, 30°C; and YP+7% glycerol, 30°C). The bottom left hand side horizontal bar chart displays the total number of significant interactions for each condition tested. The top vertical bar chart displays the number of interactions unique or shared between conditions indicated by a black dot in the bottom chart box. Unique interactions are represented by a single black dot between all 5 conditions tested. Several dots connected with a black line represent the number of interactions shared in the selected conditions. (**B**) Heatmap depicting fold change of 86 ncRNA interactions that display significant change in the five conditions tested compared to rich medium. Specific interactions are arranged on the y-axis. Conditions are displayed on the x-axis. Negative

interactions are represented as shades of blue. Positive interactions are represented as shades of yellow. **c** Visual representation of fitness for selected single and double deletion mutants in the indicated conditions.

FIG. 5. Area proportional Venn diagrams displaying unique and shared interactions between SNR17A and SNR17B. Unique and shared interactions between SNR17A and SNR17B (q<0.1) are displayed in (**A**) YPD, 30°C; (**B**) YPD, 37°C; (**C**) YP+7% Glycerol, 30°C; (**D**) YPD+1 M NaCl, 30°C and (**E**) YPD+4 mM H_2O_2, 30°C. Light grey (centre) – shared interactions between SNR17A and SNR17B; mid grey (left) – unique interactions to SNR17A; dark grey (right) – unique interactions to SNR17B.

FIG. 6. Relative expression levels of SNR17A and SNR17B measured by RT-qPCR. (**A**) RNA levels measured in haploid WT strains BY4741 and Y7092, and in the natural diploid strain 96.2 in YPD, 30°C. (**B**) RNA levels measured in BY4741 under different conditions: YP+7% glycerol, 30°C; YPD, 37°C; YPD+1 M NaCl, 30°C and YPD+4 mM H_2O_2, 30°C. **c** relative expression of SNR17A and SNR17B in the SNR17AΔ and SNR17BΔ mutants in YPD, 30°C. The expression of snoRNAs in the deletion mutants was compared to the expression in the BY4741 background. The expression of SNR17B is significant higher (***p <0.001) in the SNR17AΔ strain compared to the WT strain. The relative quantities of SNR17A and SNR17B were calculated by the ΔΔCt method using *ACT1* as reference. Error bars represent standard deviation.

FIG. 7. Analysis of 18S rRNA concentrations in WT, SNR17AΔ, SNR17BΔ, SUT480Δ and SNR17AΔ/SUT480Δ. Concentrations of 18S rRNA in the WT and deletion mutants was analysed using the Tapestation 2200 system. (**A**) Comparison of 18S concentration for the WT, SNR17AΔ and SNR17BΔ in 5 different conditions. (**B**) Analysis of 18S concentrations in the SUT480Δ and SNR17AΔ/SUT480Δ mutants in two conditions.

SUPPORTING FIGURES

FIG. S1. Query strain selection for SGA. Heat-map of the solid fitness of ncRNA deletion strains used as query strains in the SGA. (**A**) Fitness of haploid deletion strains based on colony size normalized to WT. (**B**) Competitive fitness of diploid heterozygous ncRNAs grown under chemostat culture conditions. Rows represent the different growth conditions and columns

represent the ncRNAs deletions. The colour legends represent the colony size normalized to the WT (**A**) and the difference of growth of the mutants between the end and the start of the competition (**B**). Fitness reduction or increase is represented as shades of red or green, respectively. The data were taken from (*15, 16*).

FIG. S2. Heatmap depicting 2-fold change of 395 ncRNA double ncRNA deletions that shared genetic interactions between five environmental conditions tested. Deletion mutants are arranged on the y-axis and conditions are displayed on the x-axis. Negative interactions are represented as shades of blue and positive interactions are represented as shades of yellow.

FIG. S3. Scatter plot displaying correlation between fitness and the number of interactions. Number of interactions were correlated with the fitness changes in (**A**) YPD, 30°C, (**B**) YPD, 37°C, (**C**) YP+7% glycerol, 30°C and (**D**) YPD+4 mM H_2O_2, 30°C.

FIG. S4. Genetic and physical interactions in environmental conditions. Pie chart representation of genetic and physical interactions analysed between the neighbouring genes of the significantly interacting ncRNAs**.** Dark blue colour in the larger pie charts represents the percentage of ncRNAs protein-coding neighbouring genes with a significant type of interactions. Smaller pie charts display the proportion of these interactions broken down into genetic (mid blue) and physical interactions (light blue) in YPD, 30°C; YPD, 37°C; YP+7% glycerol, 30°C; YPD+1 M NaCl, 30°C; and YPD+4 mM H_2O_2, 30°C.

FIG. 5. Spot assay to determine growth differences between SNR17A and SNR17B deletion strains. Serial dilutions (2x for **A**, and 10x for **B** to **E**) of three biological replicates of haploid SNR17AΔ and SNR17BΔ mutants along with a host strain Y7092 were spotted on YPD, 30°C (**A**), YPD, 37°C (**B**), YP+7% glycerol, 30°C (**C**), YPD+4 mM H_2O_2, 30°C (**D**) and YPD+1 M NaCl, 30°C (**E**). Growth was recorded after 24h.

FIG. S6. Area proportional Venn diagrams displaying unique and shared interactions between SNR17A and SNR17B at different q-values. Unique and shared interactions between SNR17A and SNR17B are displayed at $q<0.01$ and <0.001. (**A**) SGA data in YPD, 30°C; (**B**) YPD, 37°C; (**C**) YP+7% Glycerol, 30°C; (**D**) YPD+1 M NaCl, 30°C and **e** YPD+4 mM H_2O_2, 30°C. Light

grey (centre) – shared interactions between SNR17A and SNR17B; mid grey (left) – unique interactions to SNR17A; dark grey (right) – unique interactions to SNR17B.

FIG. S7. SUT480 does not altered SNR17A and SNR17B RNA levels. RNA levels of SNR17A and SNR17B were analysed in the SUT480 deletion mutant in BY4741 (**A**) and Y9072 background (**B**). Quantification of the RNA levels of SUT480 in *SNR17AΔ* and *SNR17BΔ* strains was also carried out (**C**). mRNA levels of *RNH202* in a SUT480Δ deletion in BY4741 and Y7092 strains (**D**). RNA was collected in YPD at 30ºC, RNA levels were quantified by RT-qPCR and compared using t-test or ANOVA

FIG. S8. Construction and validation of query strains. (**A**) Strategy to construct and validate ncRNA query deletion mutants. Briefly, ncRNA deletion cassette composed of the natMX4 marker and ncRNA complementary flanking regions were transformed into the MATα strain (Y7092) to delete the ncRNAs of interest. Following transformation, single colonies were PCR validated with primer sets: (i) confA + confNatR, (ii) confNatF + confD and (iii) confA + confB. Primer sets (i) and (ii) only amplified PCR bands if the deletion cassettes were integrated at the correct loci. Primer set (iii) amplified a PCR band if no integration event occurred. (**B**) Agarose gel electrophoresis for the PCR validation of randomly selected ncRNA query mutants. U: upstream flank PCR with primer set confA + confNatR; D: downstream flank PCR with primer set confNatF + confD; N: control PCR for the native ncRNA, with primer set confA + confB; M: 1 kb New England Biolabs ladder.

FIG. S9. Validation of a subset of SGA double deletion mutants. (**A**) Strategy to validate the double ncRNA deletion mutants. Following SGA, randomly selected double deletion haploid mutants were subjected to confirmation PCR. Primer sets (i) confA + confKanR and (ii) confKanF + confD were used to test for the *kanMX4* deletion cassette integrations. Primer sets (iii) confA + confNatR and (iv) confD + confNatF were used to test for the *natMX4* deletion cassette integrations. Primers confA + confB provided additional ncRNA deletion confirmation, only amplifying bands if the ncRNAs were intact. (**B**) Agarose gel electrophoresis for PCR validation on a selection of mutants. U: upstream flank PCR with primer set confA + kanB or confNatR; D: downstream flank PCR with primer set kanC or confNatF + confD; N: control PCR for the native ncRNA with primer set confA + confB. M: 1 kb New England Biolabs ladder.

Fig. 1

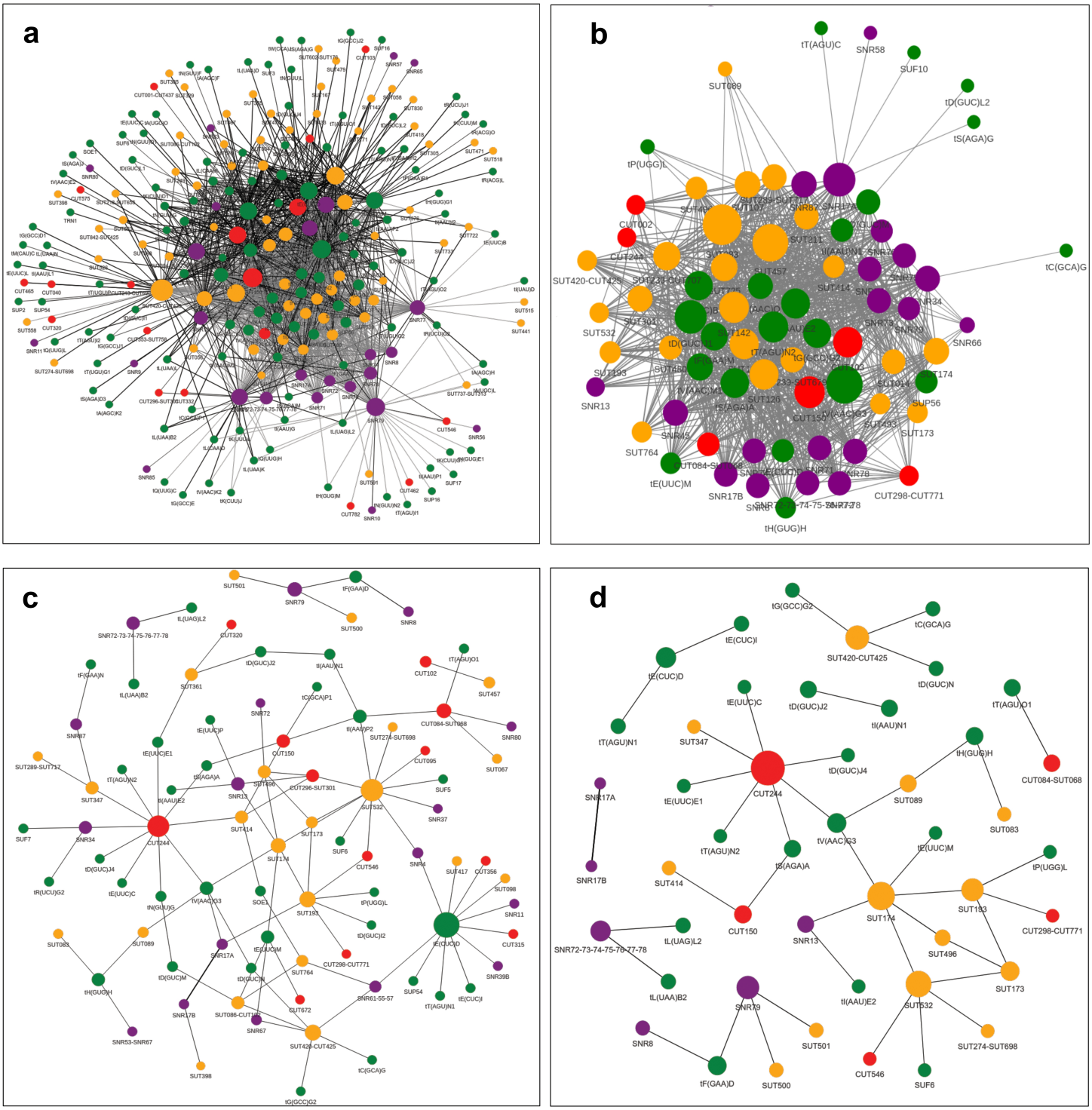
a
b
tT(AGU)C
SNR58
SUF10
SUT089
tD(GUC)L2
tS(AGA)G
tP(UGG)L
CUT002
tC(GCA)G
SUT420-CUT425
SUT532
SNR66
SUT193
SNR13
SUP56
SUT173
SUT764
tE(UUC)M
SNR17B
CUT298-CUT771
tH(GUG)H
c
SUT501
SNR79
tF(GAA)D
SUT500
SNR8
tL(UAG)L2
SNR72-73-74-75-76-77-78
CUT320
tD(GUC)J2
tI(AAU)N1
tT(AGU)O1
CUT102
SUT457
tF(GAA)N
tL(UAA)B2
SUT361
tC(GCA)P1
SNR72
CUT084-SUT068
SNR80
SNR87
tE(UUC)P
tI(AAU)P2
SUT274-SUT698
tE(UUC)E1
CUT150
CUT095
SUT067
SUT289-SUT717
tT(AGU)N2
tS(AGA)A
SUT496
CUT296-SUT301
SUT5
SUT347
tI(AAU)E2
SNR13
SUT532
SNR37
SUF7
SNR34
CUT244
SUT414
SUT173
SUF6
tD(GUC)J4
SUT174
CUT546
SNR4
SUT417
CUT356
tR(UCU)G2
tE(UUC)C
SUT098
tN(GUU)G
tV(AAC)G3
SOE1
SUT193
tP(UGG)L
SNR11
SUT083
SUT089
tD(GUC)I2
tE(CUC)D
CUT315
SNR17A
tE(UUC)M
CUT298-CUT771
tD(GUC)M
tD(GUC)N
SUT764
SNR39B
tH(GUG)H
SNR61-55-57
SUP54
tE(CUC)I
tT(AGU)N1
SNR17B
SUT086-CUT102
CUT672
SNR67
SNR53-SNR67
SUT420-CUT425
tC(GCA)G
SUT398
tG(GCC)G2
d
tG(GCC)G2
tC(GCA)G
tE(CUC)I
SUT420-CUT425
tE(CUC)D
tD(GUC)N
tE(UUC)C
tD(GUC)J2
tI(AAU)N1
tT(AGU)O1
tT(AGU)N1
SUT347
tH(GUG)H
tD(GUC)J4
CUT084-SUT068
SNR17A
tE(UUC)E1
CUT244
SUT089
SUT083
tV(AAC)G3
tE(UUC)M
tT(AGU)N2
tS(AGA)A
tP(UGG)L
SNR17B
SUT414
SUT174
SUT193
CUT150
CUT298-CUT771
SNR72-73-74-75-76-77-78
tL(UAG)L2
SNR13
SUT496
SUT173
tL(UAA)B2
SNR79
tI(AAU)E2
SUT532
SNR8
SUT501
SUT274-SUT698
tF(GAA)D
SUT500
CUT546
SUF6

Fig. 2

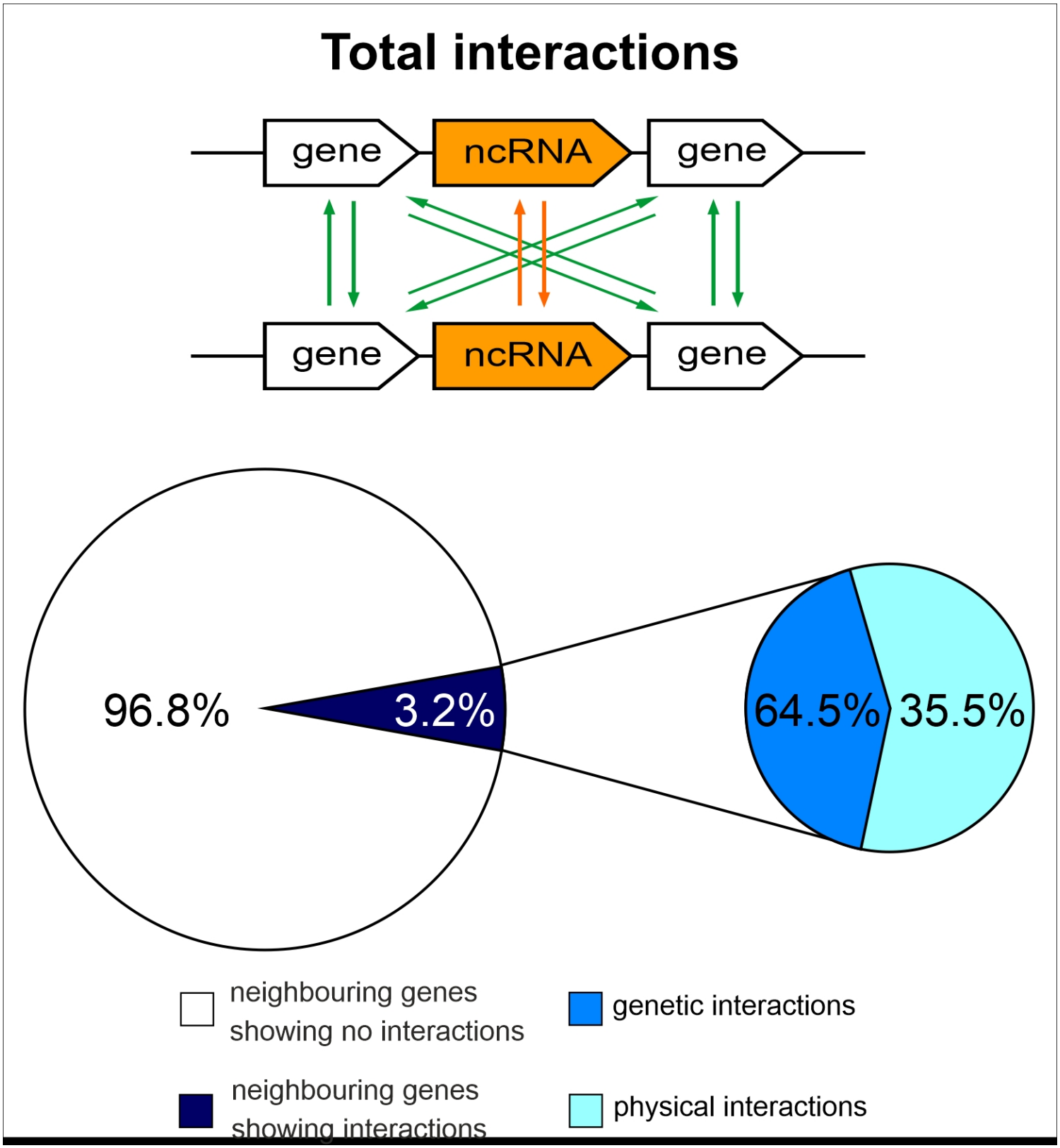
Total interactions
gene
ncRNA
gene
gene
ncRNA
gene
96.8%
3.2%
64.5%
35.5%
neighbouring genes showing no interactions
genetic interactions
neighbouring genes showing interactions
physical interactions

Fig. 3

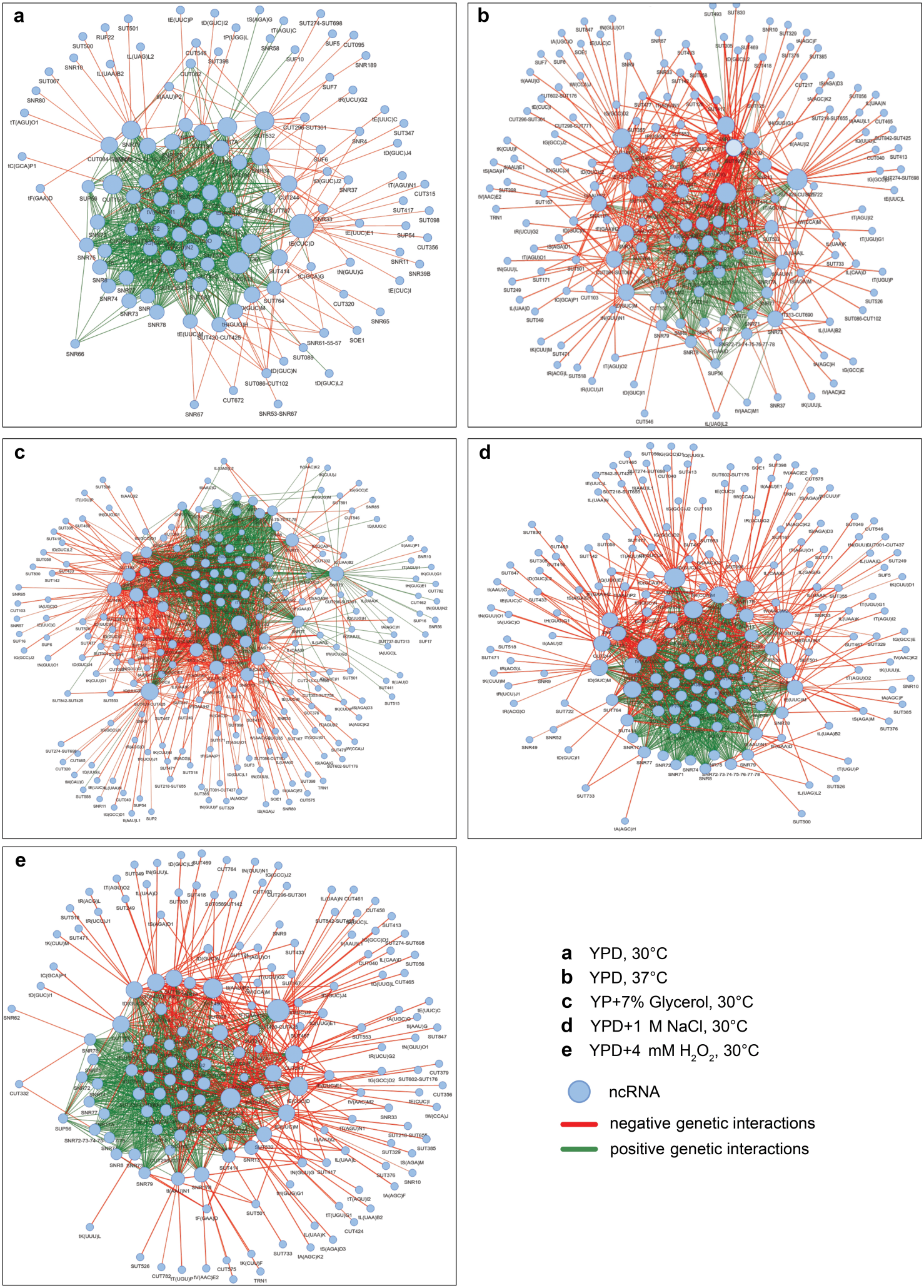
a
b
c
d
e
a YPD, 30°C
b YPD, 37°C
c YP+7% Glycerol, 30°C
d YPD+1 M NaCl, 30°C
e YPD+4 mM H_2O_2, 30°C
ncRNA
negative genetic interactions
positive genetic interactions

Fig. 4

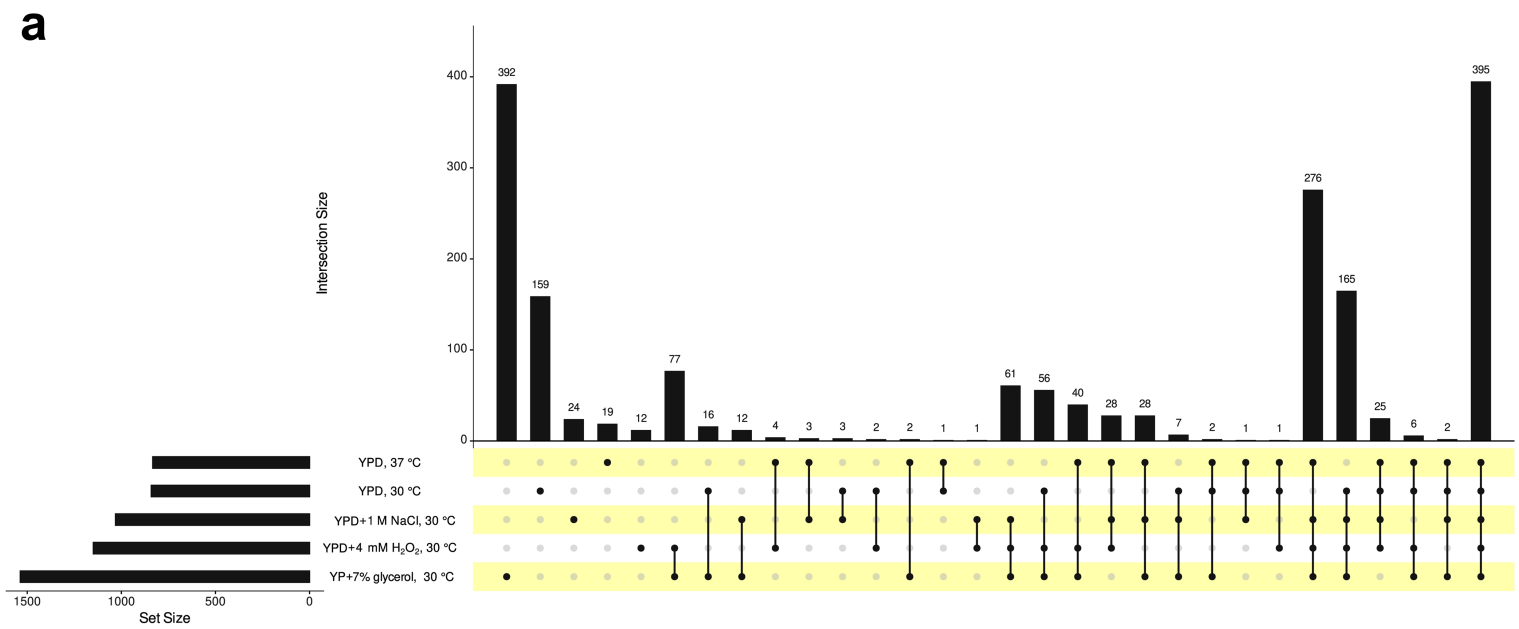
a
Intersection Size
Set Size
YPD, 37 °C
YPD, 30 °C
YPD+1 M NaCl, 30 °C
YPD+4 mM H2O2, 30 °C
YP+7% glycerol, 30 °C
392
159
24
19
12
77
16
12
4
3
3
2
2
1
1
61
56
40
28
28
7
2
1
1
276
165
25
6
2
395

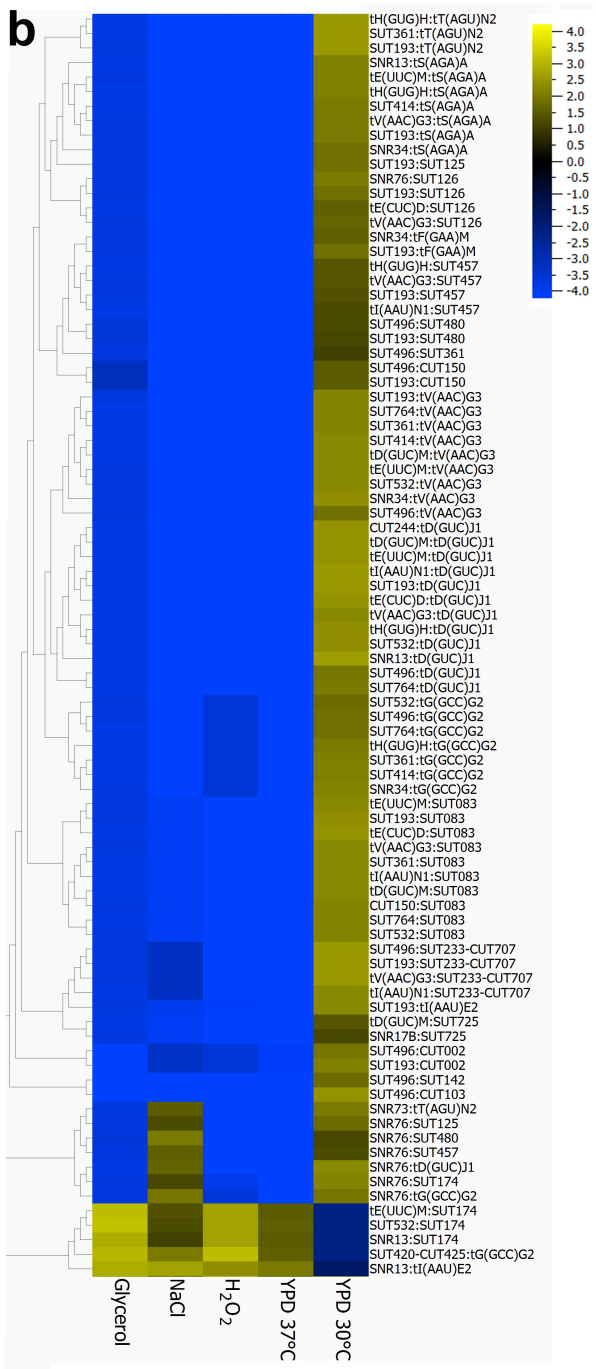
b
Glycerol
NaCl
H2O2
YPD 37°C
YPD 30°C

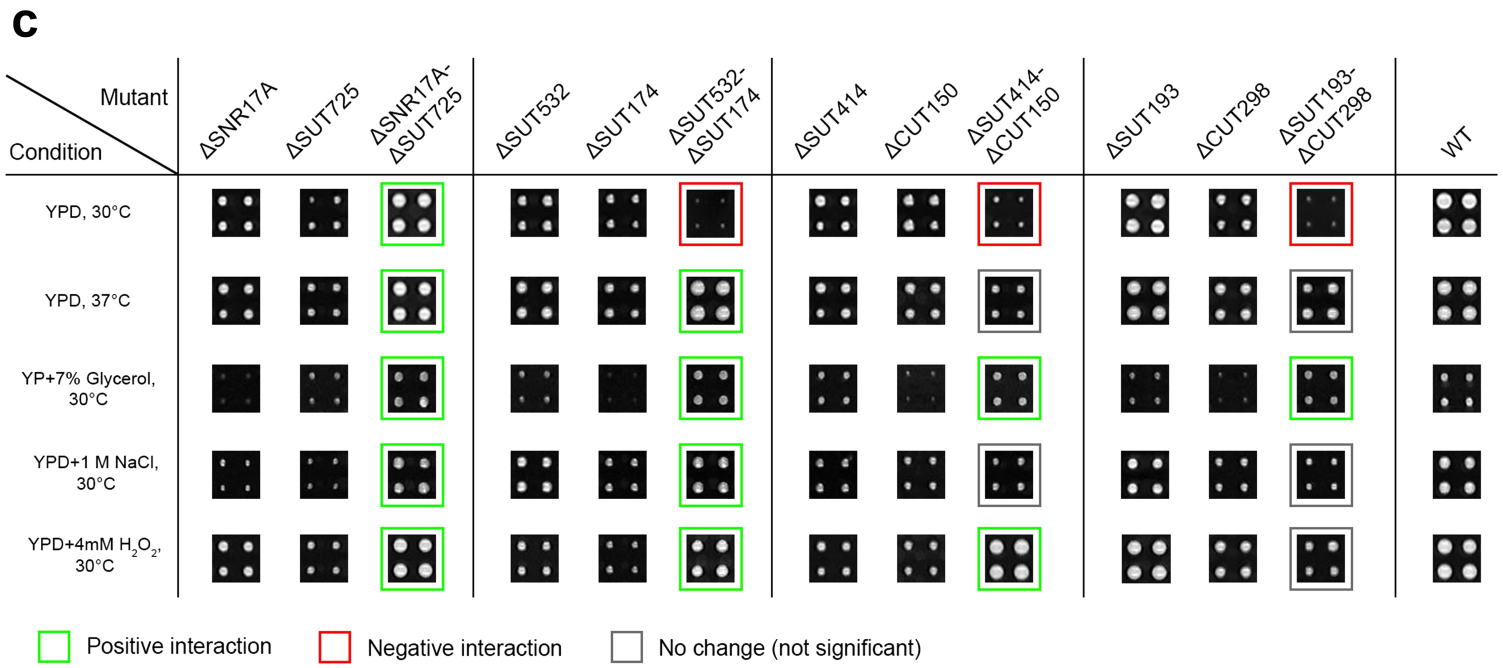
c
Mutant
Condition
ΔSNR17A
ΔSUT725
ΔSNR17A-ΔSUT725
ΔSUT532
ΔSUT174
ΔSUT532-ΔSUT174
ΔSUT414
ΔCUT150
ΔSUT414-ΔCUT150
ΔSUT193
ΔCUT298
ΔSUT193-ΔCUT298
WT
YPD, 30°C
YPD, 37°C
YP+7% Glycerol, 30°C
YPD+1 M NaCl, 30°C
YPD+4mM H2O2, 30°C
Positive interaction
Negative interaction
No change (not significant)

Fig. 5

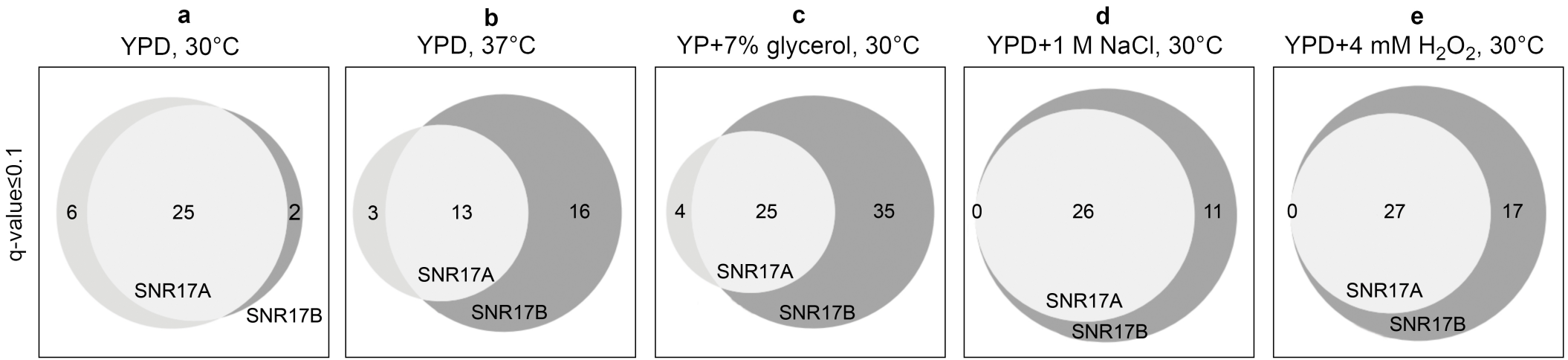
a
YPD, 30°C
b
YPD, 37°C
c
YP+7% glycerol, 30°C
d
YPD+1 M NaCl, 30°C
e
YPD+4 mM H_2O_2, 30°C
q-value≤0.1
6
25
2
SNR17A
SNR17B
3
13
16
SNR17A
SNR17B
4
25
35
SNR17A
SNR17B
0
26
11
SNR17A
SNR17B
0
27
17
SNR17A
SNR17B

Fig. 6

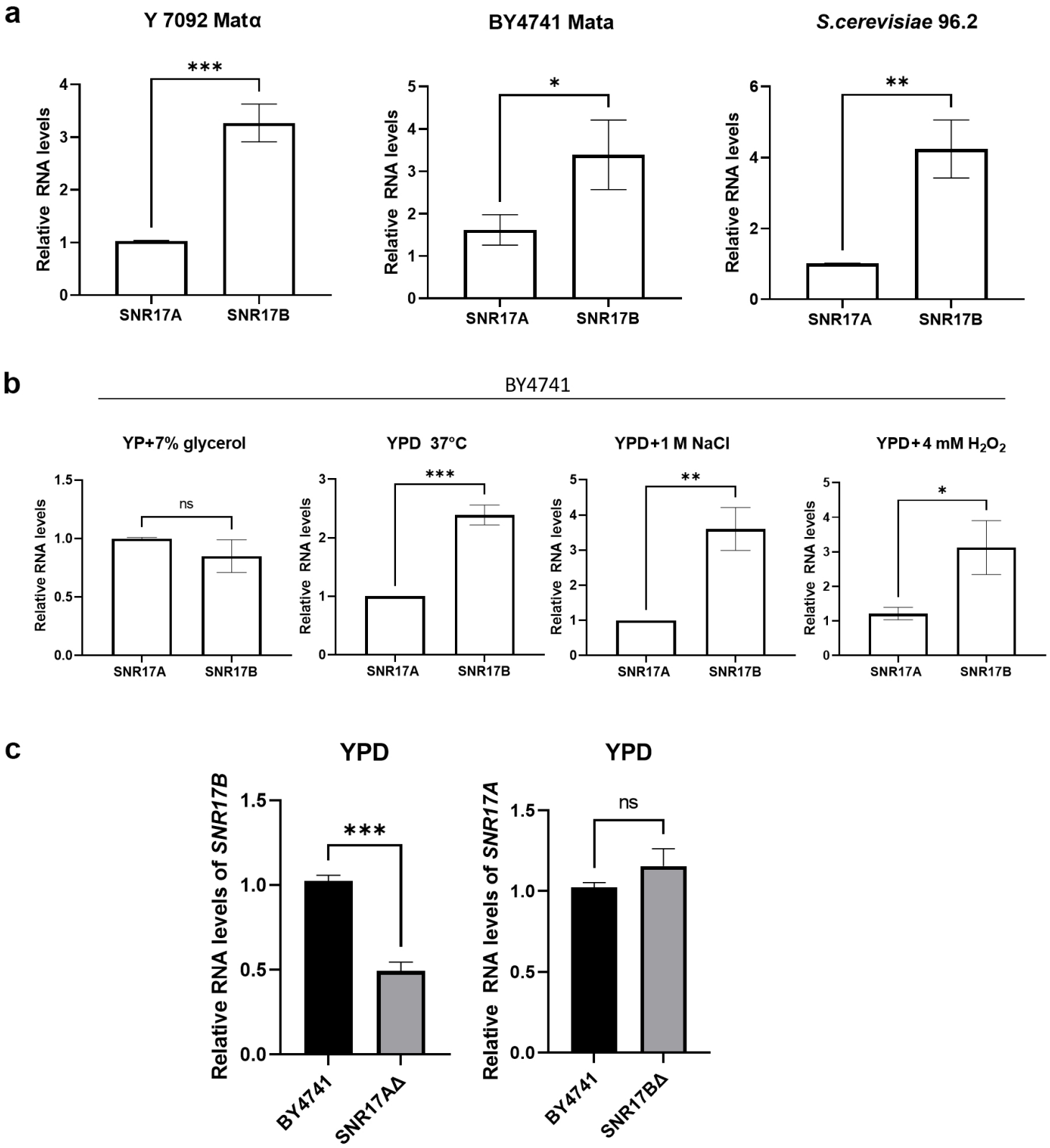
a
Y 7092 Matα
BY4741 Mata
S.cerevisiae 96.2
Relative RNA levels
SNR17A
SNR17B
***
*
**
b
BY4741
YP+7% glycerol
YPD 37°C
YPD+1 M NaCl
YPD+4 mM H2O2
ns
c
YPD
Relative RNA levels of SNR17B
Relative RNA levels of SNR17A
BY4741
SNR17AΔ
SNR17BΔ

Fig. 7

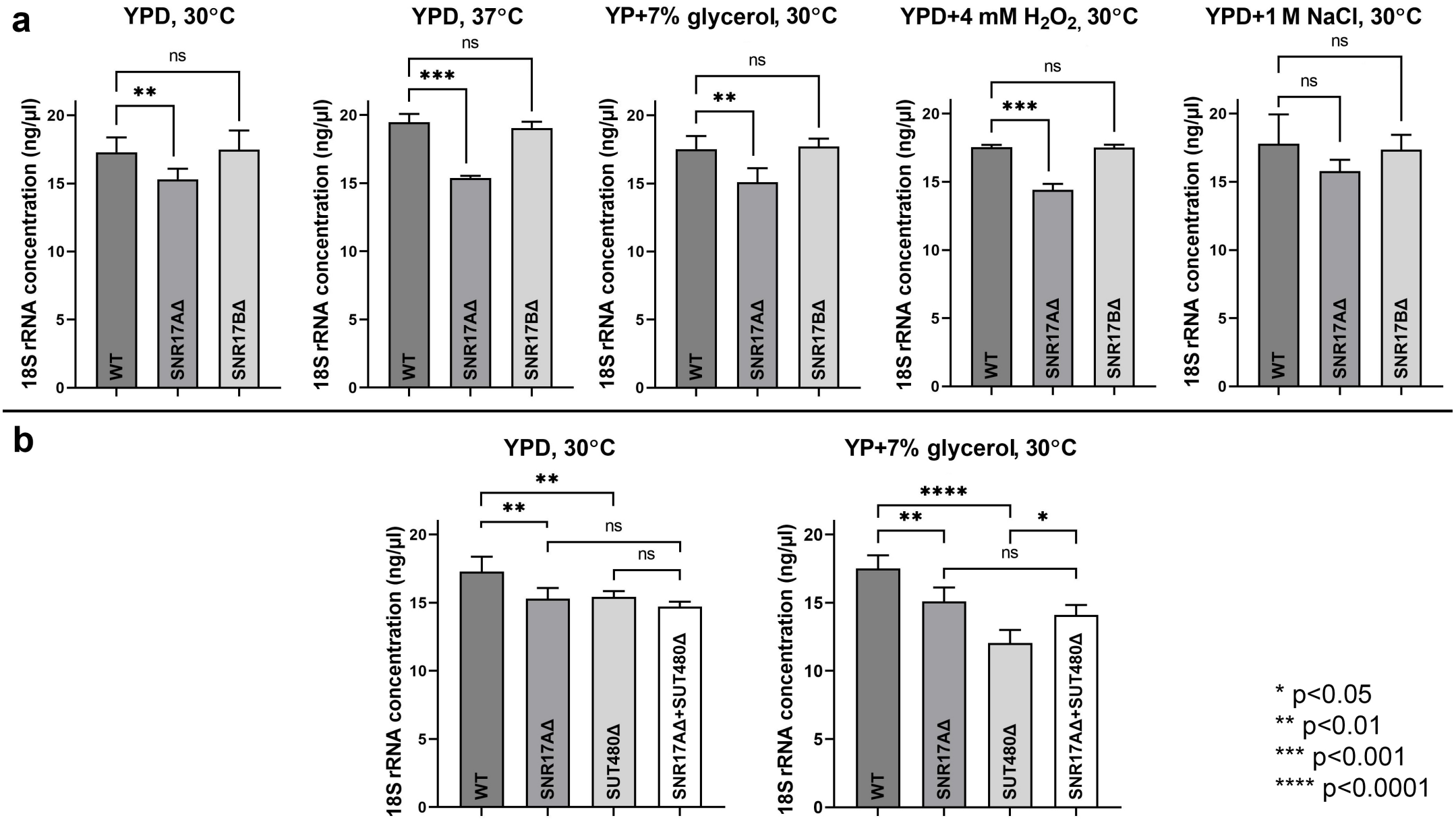
a
YPD, 30°C
YPD, 37°C
YP+7% glycerol, 30°C
YPD+4 mM H2O2, 30°C
YPD+1 M NaCl, 30°C
18S rRNA concentration (ng/µl)
WT
SNR17AΔ
SNR17BΔ
ns
**
***
b
YPD, 30°C
YP+7% glycerol, 30°C
SUT480Δ
SNR17AΔ+SUT480Δ
****
*
* p<0.05
** p<0.01
*** p<0.001
**** p<0.0001

Links to Supplementary Materials

(GitHub: https://github.com/Sookie-S/SGA-analysis)

Supplementary Dataset S1
Supplementary Dataset S2
Supplementary Dataset S3
Supplementary Dataset S4
Supplementary Dataset S5
Supplementary Dataset S6
Supplementary Dataset S7
Supplementary Dataset S8

Supplemetary Table S1

Supplemetary Fig. 1
Supplemetary Fig. 2
Supplemetary Fig. 3
Supplemetary Fig. 4
Supplemetary Fig. 5
Supplemetary Fig. 6
Supplemetary Fig. 7
Supplemetary Fig. 8
Supplementary Fig. 9